Thermally stimulated luminescence and other related processes in pre-irradiated rare gas solids

Alexey N.Ponomaryov

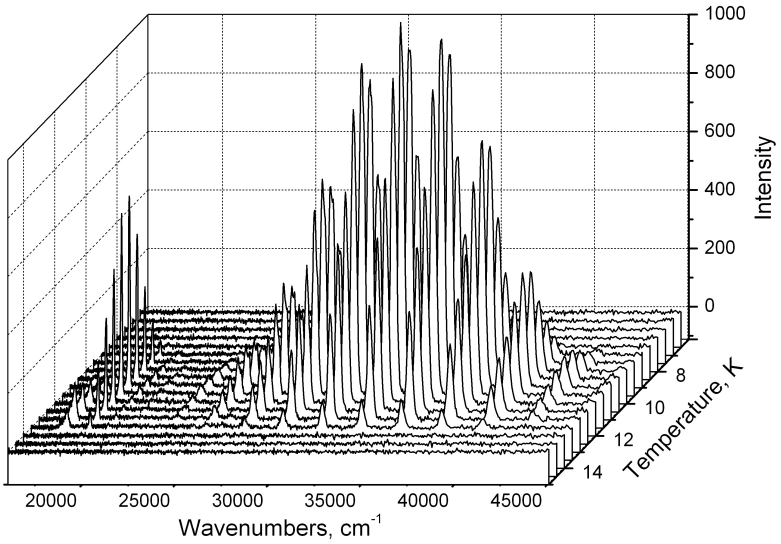

Dissertation

Technische Universität München

Technische Universität München

Institut für Physikalische und Theoretische Chemie

Thermally stimulated luminescence and other related processes in pre-irradiated rare gas solids.

Alexey N. Ponomaryov

Vollständiger Abdruck der von der Fakultät für Chemie

der Technischen Universität München zur Erlangung des akademischen Grades eines

Doktors der Naturwissenschaften

genehmigten Dissertation.

Vorsitzender: Univ.-Prof. Dr. K. Köhler

Prüfer der Dissertation:

1. Univ.-Prof. V.E. Bondybey, Ph.D. (Univ. of California, Berkeley, USA), i.R.
2. Univ.-Prof. Dr. R. Niewa

Die Dissertation wurde am 13.06.2007 bei der Technischen Universität München eingereicht und durch die Fakultät für Chemie am 17.07.2007 angenommen.

to my Parents,

my brother and sister

"The stars are beautiful, because of a flower that cannot be seen."

Little Prince.

Antoine de Saint-Exupéry

"The Little Prince."

Contents

1. Introduction

"If rare gas crystals did not actually exist,
condensed matter theorists would have
invented them."
K.S. Song. [1].

Spectroscopists and solid state physicists are likely to agree that Rare Gas Solids (RGS) play an important role in molecular and condensed matter sciences today. The history of the RGS started at the beginning of the 20^{th} century, even though helium was identified as a new element in the spectrum of the Sun some 25 years earlier. Argon, neon, krypton and xenon were discovered in the Earth's atmosphere by the end of the 19^{th} century [2, 3]. Interestingly, the fact that rare gas solids may provide a suitable medium for spectroscopic studies was discovered very shortly after their discovery. Vegard started already in the early 1920's a series of studies, which would clearly fall into the area which is today called "*matrix isolation*".

After a gap of some thirty years, mainly due to the Second World War, the interest in spectroscopic studies in solid rare gases resurfaced in the early 1950's, when Pimentel coined the phrase "*matrix isolation*" [4] and when deliberate, systematic studies of species isolated in rare gas solids started [5]. The main aim of matrix isolation studies at that time was the observation and characterization of highly reactive radicals and other reaction intermediates. Such species, which otherwise under normal conditions have only a very short existence, could be stabilized in the rigid, inert solid, and then be studied at leisure by spectroscopic means. Over the next years hundreds of free radicals, molecular ions, clusters and similar transient species were generated, detected, and their molecular constants and other properties determined in rare gas matrices [6–8].

Rare-gas solids exist only at low cryogenic temperatures and that's why they are also called "*cryocrystals*". Elegantly simple, they are ordered cubic arrays of barely interacting closed shell atoms, held together only by Van der Waals forces and that's why A.F. Prikhot'ko coined for them the term "*cryocrystals*" [9]. The face centered cubic (fcc) lattice is the stable structure for solid xenon, krypton, argon and neon. In some cases of non-optimal crystal growth, a hexagonal closed-packed (hcp) phase may be found as a metastable admixture [10]. Optical experiments and band structure calculations indicated that rare gas solids possess among all substances in nature the largest forbidden energy gaps, ranging from about 9.3 eV in solid Xe to 21 eV in solid Ne [1]. This means that the RGS can be considered as model substances for insulating materials.

During the growth of RGS various kinds of defects may appear in their structure. The ideas of defects in solids were clearly formulated by the early 1950's as a result of extensive studies of ionic crystals and metals. In a pure solid [11–13] the two point defects, which are most likely to be present, are vacant lattice sites - vacancies, and atoms or molecules in interstitial sites in the lattice - the interstitials [1]. In real solids [14–19] the defects may also include impurity atoms, radicals, more complex dislocations, twins, grain boundaries and many others etc. [9]. Defects affect solid properties. The development of these ideas demonstrated that point defects played an important role in many solid state properties and processes which occur in solids. For example, in a crystal containing vacancies diffusion may occur by an interchange of the impurity atoms or molecules and vacancies. Atomic migration and hence macroscopic diffusion in solids can take place via these defects. In solids which are irradiated by some kind of ionizing radiation - X-rays, α-particles, high and low energy electrons - the ionic centers and electrons appear as an additional kind of charged defects [1]. The pre-existing and radiation induced defects play a crucial role in chemical reactivity, electrical properties and mechanical behavior.

Thus, studying point defects in solids is of prime importance for understanding the physics and chemistry of the real solids. Rare-gas solids appeared to be ideal systems for testing defect theories [20]. That is because it has been assumed that

in these systems it is a reasonable approximation to take the interatomic forces as a central, short-range and pair-wise additive.

When a rare-gas solid is exposed to high-energy radiation, part of the excitation energy may remain stored in the crystal in the form of radicals, self-trapped charge centers or charge carriers trapped in some defect sites. The amount of energy stored in the solid during irradiation may be quite appreciable, and when the crystal is allowed to gradually warm up, various processes can be "*activated*", with a part of this stored energy being released. The electrons may be promoted from shallow traps into the conduction band and neutralize positively charged ions. At higher temperatures diffusion and reactions of neutral atoms and impurities may also take place. The energy released in these processes may be manifested in various ways, for instance by emission of photons and electrons, and methods based on the observation and monitoring of these effects are often referred to as "*activation spectroscopy*".

The methods of activation spectroscopy can provide useful information and insights into the nature of the defects, and about the processes proceeding in the sample. Nevertheless, for a long time some of these methods were rarely applied for studying cryocrystals and most experiments relied on the TSL measurements. The first successful experiment on TSEE in RGS, specifically argon, was carried out in 2000 in our group [6]. In 2002 anomalous desorption in RSG induced by electron stimulation was also firstly observed in our laboratory. In earlier experiments all these phenomena were registered independently on different samples, since, as was mentioned above, these experiments are very sensitive to the structure of the crystals, this had to be taken into account and made interpretation more difficult. But this problem could be solved by developing a special apparatus where all the parameters needed for the interpretation of these processes could be measured simultaneously.

Quite recently we have developed such an experimental setup which provided most of the parameters which were needed for better understanding processes taking place in the rare-gas solids: temperature of the substrate on which the sample is grown; pressure in the vacuum chamber, emission of the electrons and total yield

of photons in vacuum UV range or spectrally resolved in UV, visible and near IR ranges. A special software had to be developed too, for the measurements and analysis of the data.

References

[1] Song and Williams, *Self-Trapped Excitons, Springer Series in Solid State Science*, Springer-Verlag, textit105, Berlin, **1996**.

[2] W.H. Keesom, *Helium*, Elsevier, New York, **1942**; reprinted without revision, **1959**.

[3] M.W. Travers, *Discovery of the rare gases*, Edward Arnold, London, **1928**.

[4] E. Whittle, D.A. Dows and G.C. Pimentel, *J.Chem.Phys.*, **1954**, *22*, 11, (1943).

[5] V.E. Bondybey, E.V. Savchenko, *Fizika Nizkikh Temperatur*, September-October **2000**, *26*, Nos. 9/10, special issue.

[6] D.H.Levy, L.Whartson and R.E. Smalley, *Acc.Chem.Res.*, **1977**, *10*, 139.

[7] T.A. Miller, B.R. Zagarski, T.J. Sears and V.E. Bondybey, *J.Phys.Chem.*, **1980**, *84*, 3154.

[8] V.E. Bondybey, *Science*, **1985**, *227*, 125.

[9] A.F. Prikhot'ko, *Cryocrystals*, Naukova Dumka, Kiev, **1983**.

[10] J.A. Beattie, G.A. Cook W.F. Edgell et.al., *Argon, helium and the rare gases*, New York, **1961**, *1*.

[11] M. Kirm, H. Niedrais, *J. Luminescence*, **1994**, *60-61*, 611.

[12] A.N. Ogurtsov, E.V. Savchenko, O.N. Grigorashchenko, S.A. Gubin, I.Ya. Fugol', *Low Temp. Phys.*, **1996**, *22*, 922.

[13] M. Kink, R. Kink, V. Kisand, J. Maksimov, M. Selg, *Nucl. Instr. and Meth. B*, **1997**, *122*, 668.

[14] M.E. Fajardo, V.A. Apkarian, *J. Chem. Phys.*, **1988**, *89*, 4124.

[15] A.V. Danilychev, V.A. Apkarian, *J. Chem. Phys.*, **1993**,*99*, 8617.

[16] R. Dersh, B. Herkert, M. Witt, H.-J. Stockmann, H. Ackermann, *Z. Phys. B: Condens. Matter*, **1990**, *80*, 39.

[17] A. Schrimpf, C. Boekstiegel, H.-J. Stockmann, T. Bornemann, K. Ibbeken, J. Kraft, B. Herkert, *J. Phys. Condens. Matter*, **1996**, *8*, 3677.

[18] J. Becker, O.N. Grigorashchenko, A.N. Ogurtsov, M. Runne, E.V. Savchenko, G. Zimmerer, *J.Phys.D, Appl. Phys.*, **1998**, *31*, 749.

[19] L. Khriachtchev, M. Petterson, S. Pehkonen, E. Isoniemi, M. Rasanen, *J. Chem. Phys.*, **1999**, *11*, 1650.

[20] E.V. Savchenko et.al., *Surface Science*, **2002**, *507-510*, 754-761.

2. Theory and Methods of Analyzing

2.1. Rare Gas Solids

2.1.1. Introduction

The subject of the current dissertation involves experiments carried out in our laboratory on samples of solidified rare gases. These materials possess a number of interesting properties, and form from the scientific point of view a very attractive subject for experimental or theoretical considerations, in view of their specific, interesting properties. The entire family of rare gases represents a relatively recent addition to the periodic table, with their discovery dating only to the turn of the 20^{th} century. In the little more than 100 years elapsed since the discovery, these materials have been extensively studied, and it seems therefore reasonable to start this theses by a rapid look at their relatively brief history, and a short review of their interesting properties.

2.1.2. Discovery of the Rare Gases

During an eclipse of the Sun which occurred on August 18, 1868, in the time of the early days of spectroscopy, the sun's chromosphere was for the first time observed and investigated with the help of spectroscopes. Therefore it happened that six different observers almost simultaneously noted an intense yellow line in the spectrum, which was close in wavelength to the D_1 and D_2 Fraunhofer lines of sodium [1]. One of the observers, P.J.C. Janssen, was so struck by the brilliancy and prominence of this line, that he became convinced that it should be possible to observe it even in the absence of an eclipse, and indeed, 17 days later he succeeded in accomplishing this. Just a few weeks later, on October 20, 1868, an English astronomer W.J.S. Lockyer, who became aware of this problem, was able to show that the new yellow line was

different and more "*refrangible*" than the D_1 and D_2 sodium lines. To differentiate it from D_1 and D_2, it was called D_3 [2]. The first suggestion that the line might be caused by a new element in the solar atmosphere was made by G.Rayet [1]. Lockyer proved that the D_3 line was not caused by hydrogen, but apparently came from an element not known at that time. They called this new element "*helium*" from the Greek word "*helios*", meaning "*Sun*".

The discovery of "*inert gases*" - other elements belonging to the same group as helium in the earth's atmosphere was the result of the work of two researches, Lord Rayleigh and Sir William Ramsay. In 1882, Lord Rayleigh began an investigation of the densities of oxygen and hydrogen. Having developed elaborate equipment and techniques for measuring gas densities, he determined the density of nitrogen from several different sources. To his surprise, he found that nitrogen prepared from ammonia was always less dense by about five parts per thousand than nitrogen prepared from air by removal of oxygen, carbon dioxide, and moisture.

In 1892, Rayleigh wrote a letter to the editors of Nature asking readers for an explanation for the two kinds of nitrogen [4]. In the letter he himself offered four possible explanations:

- the nitrogen prepared from air might still contain some oxygen;
- the nitrogen prepared from ammonia might be contaminated with small amounts of hydrogen;
- the nitrogen from air might contain traces of some N_3 molecules analogous in structure to ozone;
- some of the molecules of nitrogen prepared from ammonia might have decomposed, thus decreasing the density of the gas.

Further experimentation, however, made all these explanations seem unlikely. It is at this point that Sir William Ramsay [6] began his work on the problem.

In April of 1894, Ramsay assigned his assistant, Percy Williams, the task of treating atmospheric nitrogen with heated magnesium metal and comparing the

density of the residual gas with that of the original sample of nitrogen [3]. As soon as college examinations were over, Ramsay personally took charge of the experiments. Within a short time, he was able to tell Lord Rayleigh that the residual gas was denser than atmospheric nitrogen by an amount greater than could be ascribed to experimental error. Ramsay sent a sample of the residual gas to William Crookes, a spectrographer, who identified its spectrum as being different from any of the then-known elements.

In a letter to Rayleigh, Ramsay suggested that there might be a new undiscovered gas in the sample, with on 6^{th} of August, 1894, Rayleigh answering that he also had become convinced that atmospheric nitrogen contains a new element. Subsequent experiments revealed that the new gas has to be monatomic and chemically very inert. Because of its chemical inertness, it was named by them "*argon*", "*the lazy one*" [3]. A few years later, in 1898, three new inert gases, krypton, neon and xenon, were discovered by Ramsay and Travers. Thus the rare gases became finally established as a new family in the periodic table of elements, and recognized as useful model systems both in atomic physics and in the physics of condensed matter.

Interestingly, already in 1881, the Italian scientist L. Palmieri, observed the D_3 line while making a spectroscopic examination, with gases escaping from some solid sample. He did, however, not realize that he was the first to find the new element, helium on Earth. It was not until 1895, when Ramsay heated a sample of cleveite, a uranium mineral, and sent samples of the gas evolved to Lockyer and Crookes for spectroscopic examination, that the existence of helium on Earth was finally recognized [3]. Helium gas in the Earth's atmosphere was discovered in August, 1895, this being accomplished by H.Kayser [2].

2.1.3. Solid State Properties

Since the rare gases were discovered a great variety of experiments was carried out to establish their properties. As a consequence of their valence electrons being arranged in "*closed shells*" the rare gases are chemically un-reactive and that's why they were

also named "*inert*" gases. At sufficiently low temperatures the Van der Waals forces between atoms become comparable to or larger than the thermal energies kT, and the atoms may stick together, eventually condensing to yield a liquid or solid phase. Critical constants give the condition and the highest temperature, at which gas and liquid can coexist as two distinct phases, give a useful measure of the strength of these Van der Waals forces between atoms. At the critical temperature, T_c, the densities of the gas and liquid phases become identical, so that above T_c only a single "$fluid$" phase can exist.

The forces between atoms may be represented graphically in the form of a curve showing the potential energy of two atoms as a function of the distance separating their centers. The form and appearance of this type of curve can be derived from a detailed knowledge of the properties of the individual atoms. In the case of rare gases, where the inter-atomic forces can be to a good approximation considered as arising from interaction between two induced dipoles, a useful mathematical expression is the widely used so-called Lennard-Jones potential. In this case the attractive force varies as r^{-7}, and accordingly the potential energy Φ varies with r^{-6}. At very short distances the sharply rising electrostatic repulsive forces counteract, and eventually prevail over the attraction. In this case the Lennard-Jones potential can be written in the form

$$\Phi = 4\epsilon\left[\left(\frac{\sigma}{r}\right)^{12} - \left(\frac{\sigma}{r}\right)^{6}\right] \quad (2.1.1)$$

where ϵ and σ are the depth of the potential well and the equilibrium distance at which the repulsive and attractive forces in the gas phase compensate one another. These constants are determined by the experimental results [8] and for inert gases they are given in Tab. 2.1.1. The shape of the Lennard-Jones potential curve is shown in Fig. 2.1.1, in which Φ/ϵ is plotted against r/σ.

With the knowledge of the potential energy as a function of distance r, the properties of the gaseous, liquid and solid states of the rare gases could, in principle, be calculated. However, from a practical point of view the success of these calculations is severely limited by several factors. In the first place, the above Lennard-Jones potential does not give a perfect description of the interatomic interactions,

Substance	ϵ, $\cdot 10^{-23}$ J	σ, $\mathring{A}$	Ref.
He^3	14.11	2.56	[9]
He^4	14.11	2.56	[9]
Ne	49.2	2.75	[9]
Ar	165	3.41	[10]
Kr	230	3.68	[10]
Xe	311	4.07	[10]

Tab. 2.1.1: Values of constants ϵ and σ for the Lennard-Jones (12-6) potential.

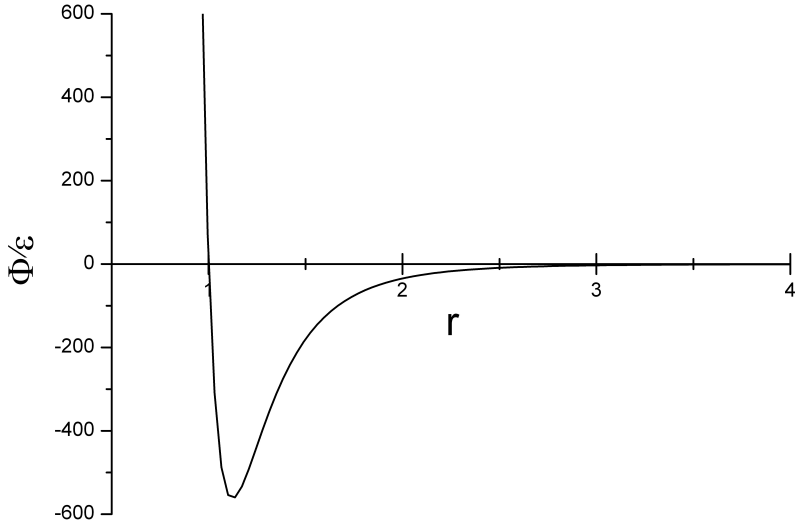

Fig. 2.1.1: Lennard-Jones (12-6) potential for Ar

the determination of the constants ϵ and σ [8] is of course subject to inaccuracies, but more importantly, the interaction of two atoms cannot be exactly described by an empirical, two constant formula. Even more importantly, the properties of a condensed phase cannot be obtained by assuming a simple addition of two-body interactions, and for a better description three-body - or generally multi-body effects would have to be considered.

The calculations made to determine the crystallographic arrangements, which might be found when the atoms condense into the solid state, lead to two preferred, low energy closely packed structures. These structures are called hexagonal closely

packed (hcp) and the face-centered cubic (fcc), respectively, and from the energetic point of view the difference between these two structures is very small. The experimental results indicate that in pure rare gas solids the fcc shown in Fig. 2.1.2, is preferred. The element specific constants a and r_m, defined in Fig. 2.1.2 are the so-

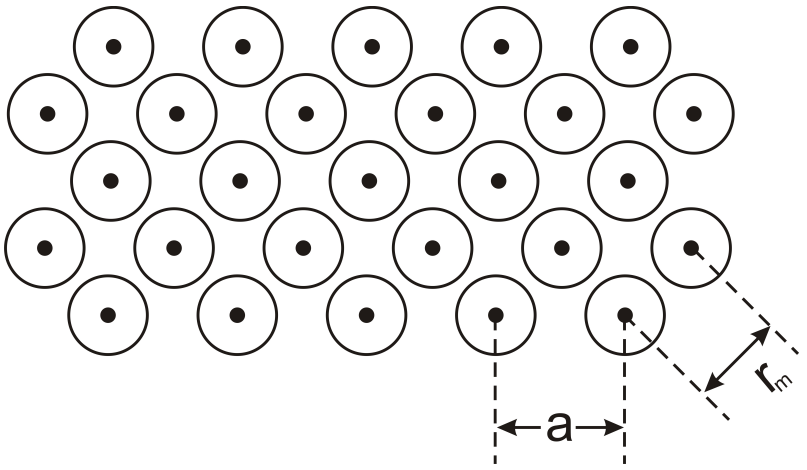

Fig. 2.1.2: Schematic presentation of the fcc structure of the rare gas solid.

called lattice constant a and the equilibrium closest neighbor interatomic distance r_m. As can clearly be seen from the drawing

$$a = r_m\sqrt{2}. \quad (2.1.2)$$

2.1.4. Structural Defects of the Rare Gas Solids

It is well known from the experiments that the real crystals of the rare gases are usually far from ideal and invariably contain a variety of defects. Several different kinds of defects may be found, and these are often very important in determining the solid properties. In pure rare-gas solids the so called point defects [7] play a very important role in different processes.

The study of point defects has been an intensive field of research for many years. The present ideas on point defects in solids were clearly formulated by the early 1950's as a result of extensive studies of ionic crystals and metals. In a pure solid the two point defects which are most likely to be present are vacant lattice sites - *the vacancies* - and/or an atom in an interstitial site in the lattice - *the interstitial*

[7]. One of the effects of such point defects is that they facilitate migration of individual atoms through the solid - and thus the macroscopic diffusion - which can take place via displacing these point defects. In a crystal containing vacancies, for example, diffusion can occur by a series of interchanges between atoms and vacancies.

The development of these ideas led to the general realization that point defects play a major role in many solid state properties. Other typical examples are electrical properties and mechanical behaviour. Since it is reasonable to suggest that the short-range interaction forces between neutral atoms in the rare gas solids are central to their properties, and to a good approximation pair-wise additive, the RGS appeared to be ideal systems for testing defect theories.

Defects in the rare gas solids can be produced in a number of ways, for instance by their irradiation by VUV light, X-rays or γ-or bombardment by charged particles. The point defects which arise in this way are sometimes called electronically induced defects, and depending on the irradiation source and energy, the excitation mechanisms can be quite different. In case of electron bombardment there are at least two possible ways of excitation depending on the irradiation energy. In case of a high-energy electron beam the excitation can appear via a physical displacement of an entire atom in the cell by the so-called "$knock - on$" mechanism. Such displacements cannot occur in case of low energy electrons, when the low mass of an electron in comparison with the atomic masses cannot be compensated by the kinetic energy. In this case the excitation and defect formation can still take place via electronic subsystems and atom ionization. Such electronically induced defects play an important role in a variety of processes, which can occur during slow warming up of the sample and we will discuss them in the following sections.

2.1.5. Formation of Electronically Induced Defects

As hinted above, the defects play an important role in the course of relaxation processes in irradiated materials. Interaction of ionizing radiation with insulators changes a set of defects and may create new types of metastable centers - self trapped

or localized charge carriers, as well as the products of radiation-induced reactions involving dopants (atoms, molecules, radicals). The basic physics of this phenomenon involves electronic excitation, and transport of the excitation energy. The mobile band excitations (free electrons, holes, excitons) cannot provoke immediately lattice destruction because their lifetime at a lattice site, τ_s, is much less than the characteristic time of atomic displacement, $\tau_D \sim \omega_D^{-1}$ (ω_D is the Debye frequency). If prompt charge neutralization does not take place, and charges are separated and trapped, the situation fundamentally changes with τ_s becoming comparable to the total lifetime τ_e of the trapped electronic excitation in the crystal. If the energy ΔE released in the vicinity of the trapped excitation on its decay or transformation is higher than the threshold energy E_d essential for the atom to be displaced to an interstitial position, a stable long-lived defect may be generated in the lattice. It should be noted that only point defects are formed on electronic excitation trapping. In the pure rare gases these are Frenkel pairs (vacancies and interstitials) with different separations between the components of genetically coupled pairs. Thus, the energy and time criteria of the electronically induced lattice defect formation (LDF) are [11]:

$$\Delta E > E_D$$

$$\tau_s >> \tau_D$$

The efficient processes of exciton self-trapping [12–14] into atomic and molecular states ($A-STE$ - atomic self-trapped exciton, and $M-STE$ - molecular self-trapped exciton) accompanied by a considerable energy release to the lattice contribute to a manifestation of this channel of electronic energy dissipation in RGS.

In [15] and [16] it was found that free excitons (FE) can be self-trapped because of exciton-phonon interaction. In RGS of "*light*" elements (like Ne) self-trapping into atomic type states ($A - STE$) prevails. It was assumed to be due to "*microcavity*" so-called "*bubble*" formation around the $A - STE$ as a result of prevailing repulsive forces between the excited electron and surrounding atoms because of negative electron affinities of solid Ne. In cryocrystals of "*heavy*" elements (solid

Xe, Kr and Ar) main channel of the exciton self-trapping is self-trapping into molecular type states ($M-STE$). In both cases an essential portion of energy is released locally in the lattice what is essential prerequisite for the lattice rearrangement.

The excited state molecular dynamic study [17] of a possible evolution of the $A-STE$ states into stable lattice defects suggested a microscopic model of $A-STE$ conversion to Frenkel pairs. The elastic deformation followed by the primary "*bubble*" formation because of the negative electron affinity of solid Ne [7] and hence prevailing repulsive forces between the excited atomic center and surrounding atoms occurs in a short-time scale. High local stresses in the lattice can induce some plastic deformation during the lifetime of the excited state. The analysis of possible plastic deformation revealed the microscopic structure of the exciton-induced defects formed via $A-STE$ in solid Ne. The structure appeared to present the second-nearest neighboring vacancy-interstitial pair. The experimental study of the exciton induced defects performed using activation spectroscopy methods [18,19] confirmed the model above suggested. An important feature of the model is the formation of defects in an excited state.

In the case of exciton self-trapping into $M-STE$ states relaxation energy is transferred to the surrounding atoms at both stages - in the excited state of the $M-STE$ and in the ground state:

$$Rg_E^* + Rg \rightarrow Rg_2^* + \Delta E^*(M-STE) \rightarrow h\nu(M-STE) + Rg + Rg + \Delta E(D) \quad (2.1.3)$$

In the specific case of solid Xe the energy release during the $M-STE$ vibronical cooling $\Delta E^*(M-STE)$ is about 0.45 eV [20] what is higher than the binding energy per atom in solid Xe (172.3 meV [7]). After the radiative transition ($h\nu$ $(M-STE)$) of the relaxed $M-STE$ to a repulsive part of the ground state potential, the excess energy ΔE(D)=0.86 eV is shared between two dimer atoms, in other words, there appear the two "*hot*" atoms with a 0.43 eV kinetic energy available for the defect creation. In accordance with this consideration, the mechanisms of exciton-induced defect creation can be classified as an "*excited state*" mechanism and a "*ground state*" one [21].

The self-trapping occurring during the lifetime of the excited state results in the formation of a molecular dimer aligned along the <110> crystallographic directions with an interatomic distance of 0.31 nm. This stage followed by the $M-STE$ formation in the on-center position is shown in Fig. 2.1.3 (a and b).

The center formed resembles a "$dumb-bell''$ configuration of the interstitial atom. Its displacement along the <110> direction to an off-center configuration (position c in Fig. 2.1.3) cannot stabilize the center. It was shown [22] that the split <100> "$dumb-bell''$ form is the only stable form of the interstitial atom in the Xe lattice. The separation between the "dumb-bells" atoms is found to be $0.86d$

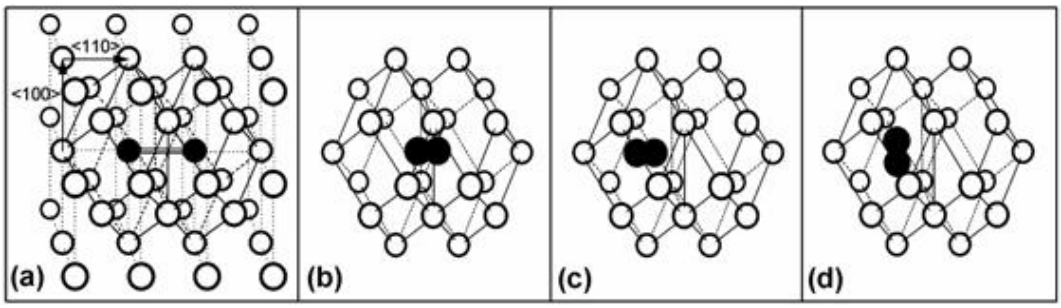

Fig. 2.1.3: Scheme of the "$excited\ state''$ mechanism of Frenkel pair formation induced by exciton self-trapping into $M-STE$ state

(d - is the distance between the nearest neighbours), which only slightly exceeds the interatomic distance between the atoms in the Xe_2^* dimer (0.31 nm). Taking this in mind, one can assume that the short-lived defect of the off-center configuration can be stabilized by the reorientation of the dimer axis to the <100> direction (d in Fig. 2.1.3). The Frank-Condon transition of this dimer to the ground state will correspond to the transition of the molecular center to the permanent defect level with almost no change in the interatomic distance. The energy needed for the reorientation can be released in the lattice in the course of the vibronic relaxation. As the theory shows [23], in a system with a strong local vibration the energy release proceeds in a jump-like multi-phonon process. It seems to be the case for the $M-STE$ relaxation what offers the basis for the development of the "$excited\ state''$ mechanism.

The model of defect creation by the "*ground state*" mechanism is not so straightforward as it may seem at first sight. The matter is that during self-trapping Rg atoms are brought closer together displacing along the <110> direction, as shown in Fig. 2.1.3 *b*. However, there are no stable interstitials of the "$dumb-bell$" configuration aligned along the <110> crystallographic direction [22]. The recent theoretical studies [24,25] showed that in the fcc lattice of RGS the weak coupling between close-packed atomic rows and the crystal matrix may give rise to an interstitial atom of a specific configuration - a smeared clump called "*a crowdion*". The vacancy also becomes delocalized, forming a smeared spared region ("*anticrowdion*").

2.2. Thermally Stimulated Luminescence

2.2.1. General Aspects

Thermoluminescence or Thermally Stimulated Luminescence (TSL) in solids is the light emission that takes place during heating of a solid following an earlier absorption of energy from radiation. It is in fact the release of energy previously absorbed and it is quit different to that which appears at high temperatures. The main condition for TSL to occur in an insulator or a semiconductor is that the material must have been previously exposed to radiation. Once TSL emission has been observed, the material will not show it again after simply cooling the specimen and reheating it, but has to be reexposed to radiation to obtain TSL again. TSL, although based on the same fundamental principles as other luminescence processes, is conventionally a misnomer since the heat radiation is only a stimulant and not an exciting agent.

The TSL was suggested as a potentially useful research tool for trap-level analyzing by Urbach in 1930 [26]. The first basic mathematical treatment of TSL was given by Randall and Wilkins in [27] and Garlick and Gibson in [28]. After that the TSL was applied in many fields of research such as: archeology, geology, health physics, medical sciences, radiation dosimetry. In 1994 it became one of the main tools for analyzing defect structures in solids [29]. Since solid rare gases are the materials with very wide energy band gap and behave as very good insulators the TSL was also applied to study them.

2.2.2. Energy-Band Model

One of the best models describing the processes leading to the appearance of TSL is "$Energy - Band\ Model$". According to this model, the trace of foreign impurities and defects responsible for luminescence in solids - called "$luminescence\ centers$" - introduced into the lattice of the host material, can be imagined to form discrete energy levels ("$donor/acceptor$" levels) within the forbidden energy gap. Other

impurities and the presence of vacant lattice sites or other lattice structural defects provide unoccupied energy levels - called "*traps*" - that have the capability of detaining ("*trapping*") the charge carriers before their recombination with the luminescent centers, thereby delaying the luminescence. Depending on the energy levels, the traps are called shallow and deep traps. The shallow traps are contributed to

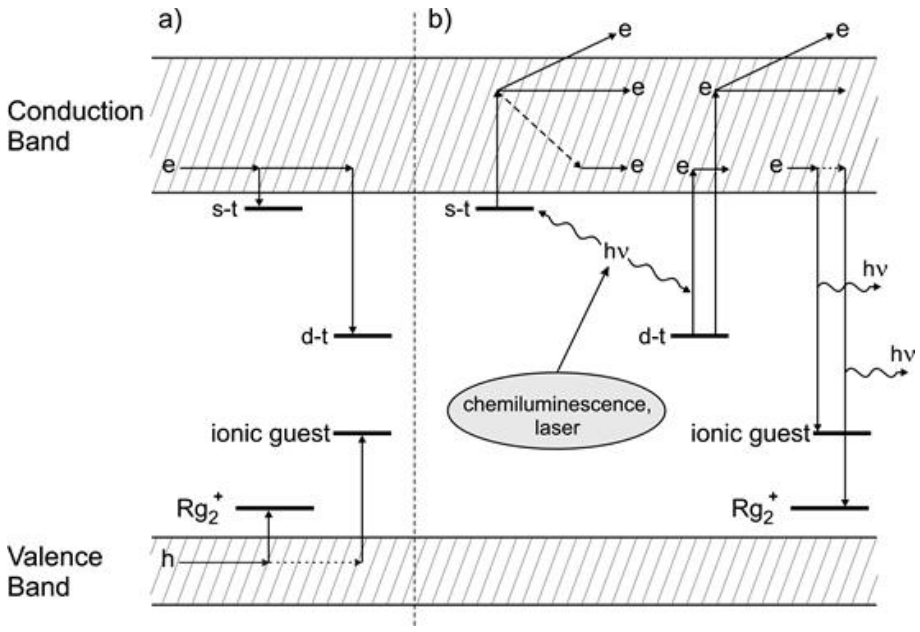

Fig. 2.2.1: Simplified schema of the Energy-Band Model

the structural defects of the sample while the deep traps belong to the impurities. These traps are denoted as electron traps and hole traps, depending on whether the trapped carriers are electrons or holes.

A simplified schematic representation of Energy-Band Model is shown in Fig. 2.2.1. During irradiation, if the luminescent center is raised to its excited state without going to the conduction band (C-band), its return to the ground state will emit fluorescence. That's why some materials (and rare gas solids as well) produce light emission while being irradiated. The wavelength of the emission depends on the nature of the luminescent center. Taking the spectra during irradiation provides information about centers formed under irradiation by the electrons and impurities presented in the sample.

On the other hand, if the electron is raised to the C-band, either from the

valence-band (V-band), or luminescent center, the electron will be free to move with much more likely possibility of its being trapped in the traps ($s-t$ - "*shallow traps*", $d-t$ - "*deep traps*"). If the electron is of luminescent center, the ionic guest is formed. Meantime, if the electron promoted from the V-band, this produces the ions of the host material. In case of RGS, this ion is Rg^+ which can recombine with neutral atom producing Rg_2^+. Holes play the same role as electrons when they are trapped and released to recombine radiatively at the recombination centers.

Once the electrons are trapped, they cannot be released without applying an additional energy. In case of shallow traps, the energy needed is in range of meV and the electrons can be freed by simply warming-up the sample. The freed electrons may recombine with ionic centers or Rg_2^+ giving the rise to TSL or the electrons can be retrapped in more deep traps. The intensity of TSL emission depends on number of the electrons released from the traps. As the temperature is raised the intensity of TSL emission increases, reaches a maximum, starts decreasing as the traps are depleted, and reduces to zero when all the traps are empty. The temperature at which the glow curve (a plot of the intensity of TSL versus temperature) exhibits a maximum is related to the trap depth E below the edge of the C-band. The area under the glow curve is proportional to the number of filled traps and hence to the amount of radiation that the material is subjected to initially. In case of deep traps ($d-t$), the electrons can be promoted to the C-band by means of light emission. The source of light can be either internal (TSL, which is also called "*chemiluminescence*") or external (such as laser). Using lasers with different wavelengths, one can study deep traps.

A single maximum in the glow curve supposes trapping levels located around a fixed energy E below the edge of C-band or above the V-band. More than one maximum in a TSL curve reveals that the traps are distributed in separate groups at different depth, each maximum representing a particular set of trapping levels. The trap depth can be calculated from knowledge of the temperature at which the maximum of TSL occurs.

Several theoretical and experiments have been carried out to modify the sim-

ple energy-band model in order to examine the phenomenon of conductivity occurring simultaneously with TSL [30–32], and for specimens showing TSL but no conductivity [33–36]. Gasiot and Fillard in 1977 [37] have also described models for the TSL process that occurs as a result of the thermal release of electrons and their recombination with trapped holes as well as the thermal release of trapped holes and their recombination with trapped electrons. More detailed description of models as they apply to TSL in various materials one can find in [38].

2.2.3. Mechanism of Thermoluminescence

The release of charge carriers from the trapping levels by thermal process depends on the probability of their escape

$$p = \frac{1}{\tau} = s \cdot e^{-\frac{E}{kT}} \quad (2.2.1)$$

where τ - is the time, the electron spend in traps; s - is the frequency factor having the dimension of reciprocal second; E - is the energy required for the release of the electron/hole at temperature T; k - Bolzman's constant. The charge carriers released from the traps on heating recombine radiatively via the C-band or V-band, giving rise to TSL whose intensity I, at any time t during heating is proportional to the rate of recombination of holes and electrons at the recombination center level, and is given by

$$I_t = I_0 \cdot e^{-pt}, \quad (2.2.2)$$

where I_0 is initial intensity at $t = t_0$, $p = s \cdot e^{-\frac{E}{kT}}$. The frequency factor s varies slowly with temperature and can be constant for a particular trap.

In practice, an electron/hole when released from the trap has a finite probability of getting retrapped. If the electrons/holes released on heating are not retrapped, and all of them recombine radiatively, the TSL intensity I_{TSL} will be proportional to the rate of release of the trapped carriers, and is given by

$$I_{TSL} = N_{t_0} \cdot s \cdot e^{-\frac{E}{kT}} \cdot e^{-\frac{s}{\beta} \cdot \int_{T_0}^{T} e^{-\frac{E}{kT}} \cdot dT}, \quad (2.2.3)$$

where N_{t_0} is the number of electrons trapped at initial temperature T_0 and β the rate of heating. Eq.(2.2.3) is the Randall and Wilkins [39, 42] expression for the first-order (monomolecular) kinetics under conditions of no retrapping.

It can be easily observed that I_{TSL} build up as the temperature increases as the second exponential term in Eq.(2.2.3) approximates unity; reaches a maximum at particular intermediate temperatures as the second term starts decreasing; and then falls off for any further increase of temperature as the second exponential decreases rapidly to reduce I_{TSL} to zero.

By setting $\frac{dT_{TSL}}{dT} = 0$ at $T = T_m$, one obtaines

$$\frac{\beta \cdot E}{kT_m^2} = s \cdot e^{-\frac{E}{kT}}$$

or

$$E = k \cdot T_m \cdot ln\frac{skT_m^2}{\beta E}. \quad (2.2.4)$$

At low temperatures, however, one gets

$$I_{TSL} = N_{t_0} \cdot s \cdot e^{-\frac{E}{kT}}. \quad (2.2.5)$$

Eq. (2.2.5) can be used to obtain the values of the traps depth E from the initial portion of the TSL curve (the so-called "*initial rise Method*") without determining s.

A graph of $ln(I_{TSL})$ against $\frac{1}{T}$ will give a straight line whose slope is equal to $\frac{E}{k}$, from which the value of E can be obtained.

From Eq.(2.2.4) it is obvious that: (i) with the increase of β (heating rate), the T_m shifts to higher temperatures for a given trap [40]; and (ii) for a constant value of β, T_m shifts toward higher temperatures as E increases or s decreases.

In case of second-order (bimolecular) kinetics [28], the released free carrier is considered to have an equal probability for going to recombination centers or returning to the same trap (retrapping). I_{TSL} can now be expressed as

$$I_{TSL} = \frac{N_{t_0}^2}{N} \cdot s \cdot exp\left(-\frac{E}{kT}\right) \cdot \left[\frac{N_{t_0}}{N} \cdot \left(\frac{s}{\beta}\right) \cdot \int_{T_0}^{T} e^{-\frac{E}{kT}} \cdot dT + 1\right]^{-2}, \quad (2.2.6)$$

where N is the total number of traps of which N_t are occupied at a time t. The second-order curve shows more TSL during the second half of the first-order curve [33]. The second-order kinetics will be exhibited by those materials in which the concentration of traps and recombination centers are almost equal. For larger concentrations of recombination centers the glow curve falls off rapidly beyond the TSL maximum conforming to the first order kinetics. The TSL curve for second-order kinetics behaves in a similar fashion as that of the first-order except that the curve is of greater half-width.

The initial rise of the TSL curve can be used for obtaining E values (when s is not known) since Eq.(2.2.6) reduces to $I_{TSL} = N_{t_0}^2 \cdot s \cdot e^{-\frac{E}{kT}}$ at low temperatures.

In case of general-order of the kinetics (where a process follows neither first-order nor second-order kinetics) the TSL intensity can be represented as

$$I_{TSL} = N_{t_0} \cdot s \cdot exp\left(-\frac{E}{kT}\right) \cdot \left[\frac{(r-1)\cdot s}{\beta} \cdot \int_{T_0}^{T} e^{-\frac{E}{kT}} \cdot dT + 1\right]^{-\frac{r}{r-1}}, \quad (2.2.7)$$

where r is the order of the kinetics, and may not be an integer value. Eq. (2.2.7) reduces to first-order (Eq. (2.2.3)) for $r = 1$, and to second-order (Eq. (2.2.6)) for $r = 2$ [45].

2.2.4. Overview of the Main Methods of Analyzing

Trapping parameters such as order of kinetics r, trap depth energy E, and the frequency factor s have appreciable influence on the TSL properties of solid. Hence, knowledge of them is of primary importance for understanding the TSL, and there have been many approaches to determining these parameters experimentally [33, 42–51]. In spite of the fact that these parameters can be experimentally determined using various techniques, there is hardly any method that is completely independent of the order of the kinetics except the initial-rise method, for which prior knowledge of the recombination kinetics is required. The TSL analysis can be meaningful only if the defect structure of the solid is known and some associated temperature-dependent parameters, such as mobility, luminescence efficiency, and band structure, are reasonably well understood.

Generally, in practice, a material does not have exhibit a single TSL peak but a multipeak curve. Before starting any analysis, the peak under investigation must be isolated from the neighboring overlapping peaks. This method of isolation is called "*cleaning technique*" and it was proposed by various researches [52, 53]. Various methods of analysis developed for obtaining TSL parameters, based on such parameters as heating rate, area measurements under the curve, glow-curve shape, curve fitting technique, and initial position of the glow-curve were developed and some of them were used in this work. So, they are described below.

Method Using Different Heating Rates As it was mentioned above, the heating rate β has a certain influence on the position of the TSL maximum T_m. Using two different rate β_1 and β_2 and finding the corresponding peak temperatures T_{m_1} and T_{m_2}, respectively, and using Eq.(2.2.4),

$$\frac{\beta \cdot E}{kT_m^2} = s \cdot e^{-\frac{E}{kT_m}}$$

one can calculate the trap depth as

$$E = \frac{kT_{m_1}T_{m_2}}{T_{m_1} - T_{m_2}} \cdot ln\left[\frac{\beta_1}{\beta_2} \cdot \left(\frac{T_{m_2}}{T_{m_1}}^2\right)\right]. \quad (2.2.8)$$

By using several heating rates, and plotting $ln(\frac{T_{m_2}}{\beta})$ versus $\frac{1}{T_m}$, a straight line is obtained with the slope $\frac{E}{k}$ and intercept $ln(\frac{E}{sk})$, from which E and s can be calculated.

Apart from being simple, this method of evaluating E is insensitive to retrapping effects, and the calculation of E is not affected by problems of thermal quenching as with the initial-rise method. Since the value of T_m is not very sensitive to changes in β, this method is approximate and results in a possible error of 20-30%. E can be obtained within 5% if the temperature measurement can be achieved within 1 K accuracy. Reliable results, however, are not obtained for overlapping peaks, since T_m is appreciably affected while peaks are isolated by the cleaning process.

Chen and Winer [54] have considered general-order kinetics to obtain an equation of the form

$$\frac{\beta E}{kT_m^2} = s \cdot \left[1 + (r-1) \cdot \frac{2kT_m}{E}\right] \cdot e^{-\frac{E}{kT_m}}, \quad (2.2.9)$$

where r is the order of the kinetics.

A plot of $ln(\frac{T_{m^2}}{\beta})$ vs. $\frac{1}{T_m}$ still yields a good value of E. The only disadvantage in this case is that one needs to know r beforehand.

Initial-Rise Method The initial-rise method can be used when the sample has a single glow curve or when there is no overlapping of glow peaks belonging to different trapping states. The method is based on the fact that as the glow curve initially begins to rise, the density of unoccupied recombination centers and the density of trapped electrons remain approximately constant, and hence the TSL intensity is strictly proportional to $e^{-\frac{E}{kT}}$.

In the case where the factor s is temperature-dependent, by the factor T^{α}, the actual trap depth will be $E - \alpha kT$.

Isothermal-Decay method Isothermal decay is a general technique for determining E and s and does not employ any particular heating cycle. The preexcited TSL material is quickly heated to a particular constant temperature and the light emission, which decays exponentially as a function of time, is monitored. This mode of heating is also called step-wise heating. The slope m of the linear plot between $ln(\frac{I_t}{I_0})$ and t will be equal to $s \cdot e^{-\frac{E}{kT}}$. The decay is observed at several temperatures and their respective slopes m are calculated. The slope of the linear plot of $ln(m)$ vs. $\frac{I}{T}$ will be $\frac{E}{k}$ and the intercept is $ln(s)$, from where E and s are calculated [55, 56].

2.2.5. Thermoluminescence-Related Phenomena

Thermally stimulated conductivity There are several phenomena which appear in solids together with TSL. Thermal detrapping of charge carriers - electrons or holes - in a preexcited solid, under the action of a direct current field applied across the layer of the material may change its conductivity if the carriers cross over to the C-band or V-band. This phenomenon is called "*Thermally Stimulated Conductivity*" (TSC). This may also give rise to TSL emission if these carriers recombine radiatively at the recombination centers. In such circumstances of detrapping, TSL and TSC will

occur simultaneously and there will be some correlation between them. In this case the methods of analysis for TSL are also suitable for TSC curves [34].

Simultaneous measurements of TSL and TSC have been carried out by various researchers [57–61]. TSC measurements may also yield useful information on the nature of defects affecting TSL and the traps and dynamics of traps and recombination centers.

However, there is at least one more related phenomenon which was studied in the current work simultaneously with TSL and needs to be explained.

Thermally Stimulated Exoelectron Emission *"Thermally Stimulated Exo − electron Emission"* (TSEE) is also an effective technique for interpreting the effects underlying TSL and for understanding the nature and distribution of the trapping states that the electrons are released from when a preirradiated sample is heated. These released electrons - called exoelectrons - get raised to the C-band. After they reach high enough energies to overcome the potential barrier at the surface and the attraction of the image charges on the surface, they leave the solid sample, and can then be collected by a detector with a positive potential electrode in place above the sample. The curve of the yield of this emission obtained as a function of temperature is also called a glow curve. The mechanism of TSEE can also be explained by Energy-Band Model, which was mentioned above, and the analysis of the TSEE curve can be done in the same way as for TSL curve. There were several researchers who have done correlated measurements of TSL and TSEE on different solids, however in the current work the first correlated measurements of TSEE and TSL on rare gas solids are presented. Moreover, in some experiments the spectrally- and time-resolved measurements of TSL were done.

References

[1] W.H. Keesom, *Helium*, Elsevier, New York, **1942**.

[2] W.J.S. Lockyer, *Nature*, **1920**, *105*, 360.

[3] J.A. Beattie, G.A. Cook, W.F. Edgell et.al., *Argon, helium and the rare gases*, New York, **1961**, *1*.

[4] L. Rayleigh, J.W.Strutt, *Nature*, **1892**, *46*, 512.

[5] M.E. Weeks, *Discovery of the Elements*, Journal of Chemical Education, Easton, Pa., **1956**.

[6] M.W. Travers, *A Life of Sir William Ramsay*, Edward Arnold, London, **1956**.

[7] K.S. Song, R.T. Williams, *Self-Trapped Excitons*, Springer Series in Solid State Science, *105*, Springer-Verlag, Berlin, **1996**.

[8] E.R. Dobbs, G.O. Jones, *Theory and properties of solid argon*, Repts. Prog. Phys., **1957**, *20*, 516.

[9] J. De Boer, *Physica*, **1948**, *14*, 139; Proc. Roy. Soc., London, **1948**, *A215*, 5.

[10] E. Whalley, W.G.Schneider, *J. Chem. Phys.*, **1955**, *23*, 1644.

[11] Ch.B. Lushchik, A.Ch. Lushchik, *Decay of electronic excitations with defect formation in solids*, Nauka, Moscow, **1989** (in Russian).

[12] I.Ya. Fugol', E.V. Savchenko, *in: Cryocrystals, eds. B. Verkin and A. Prychot'ko*, Naukova Dumka, Kiev, **1983** (in Russian).

[13] N. Schwentner, E.-E. Koch, J. Jortner, *Electronic excitation in condensed rare gases*, Springer, Berlin, **1985**.

[14] G. Zimmerer, *Excited state spectroscopy in solids*, North-Holland, Amsterdam, *1987*.

[15] G. Zimmerer, *in: Excited-State Spectroscopy in Solids, Eds. U.M. Grassano and N. Terzi*, North-Holland, Amsterdam, **1987**.

[16] I.Ya. Fugol, *Adv. Phys.*, **1988**, *37*, 1.

[17] K.S. Song, Ch.-R. Fu, *J. Low Temp. Phys.*, **1998**, *111*, 645.

[18] O.N. Grigorashchenko, V.V. Rudenkov, I.V. Khyzhniy, E.V. Savchenko, M. Frankowski, A.M. Smith-Gicklhorn, M.K. Beyer, and V.E. Bondybey, *Low Temp. Phys.*, **2003**, *29*, 876; FNT, **2003**, *29*, 1147.

[19] M. Frankowski, E.V. Savchenko, A.M. Smith-Gicklhorn, O.N. Grigorashchenko, G. Gumenchuk, and V.E. Bondybey, *J. Chem. Phys.*, **2004**, *121*, 1474.

[20] A.N. Ogurtsov, *In: E.C. Faulques et al. (eds.), Spectroscopy of Emerging Materials (NATO Science Series II. Mathematics, Physics and Chemistry)* Kluwer Academic Publishers, Dordrecht/Boston/London, **2004**, *165.*

[21] E.V. Savchenko, A.N. Ogurtsov, I.V. Khyzhniy, G. Stryganyuk, G. Zimmerer, *Phys. Chem. Chem. Phys.*, **2005**, *7*, 785.

[22] V.D.M. Doyama, R.M.J. Cotterill, *Phys. Rev.*, **1970**, *1*, 832.

[23] V. Hizhnyakov, *Phys. Rev. B*, **1996**, textit53, 13981.

[24] V.D. Natsik, E.I. Nazarenko, *Low Temp. Phys.*, **2000**, *26*, 210; *FNT*, **2000**, *26*, 283.

[25] V.D. Natsik, S.N.Smirnov, E.I. Nazarenko, *Low Temp. Phys.*, **2001**, *27*, 958; *FNT*, **27**, 1295.

[26] F. Urbach, *Ber.(IIA)*, Wien, **1930**, *139*, 353 and **1930**, *139*, 483.

[27] J.R. Randall, M.H.F. Wilkins, *Proc. Roy. Soc.*, London, **1945**, *series A 184*, 366-408.

[28] G.F.J. Garlick, A.F. Gibson, *Proc. R. Soc.*, London, **1948**, *A60*, 547.

[29] P.D. Townsend, *Radiat. Meas.*, **1994**, *23*, 341.

[30] H.J.L. Hagebeuk,P. Kivits, *Phisika*, **1976**, *83B*, 289.

[31] S.W.S. McKeever, *Thermoluminescence of Solids*, Cambridge University Press, Cambridge, **1985**, p. 8-10.

[32] A.C. Lewandowski, B.G. Markey, S.W.S. McKeever, *Phys. Rev. B: Cond. Mat.*, **1994**, *49*, 8029.

[33] R. Chen, Y. Kirsh, *Analysis of Thermally Stimulated Processes*, Pergamon, Oxford, **1981**.

[34] P. Braunlich, (Ed), *Thermally Stimulated Relaxation in Solids*, Springer-Verlag, Berlin, **1979**.

[35] A. Halperin, A.A. Braner, *Phys. Rev.*, **1960**, *117*, 408.

[36] K. Hagekyriakou, R.J. Fleming, *J. Phys. D: Appl. Phys.*, **1982**, *15*, 1795.

[37] J. Gasiot, J.P. Fillard, *J. Appl. Phys.*, **1977**, *48*, 3171.

[38] D.R. Vij,(Ed.), *Thermoluminescent Materials*, Prentice Hall, Englewood Cliffs, NJ, **1993**.

[39] J.T. Randall, M.H.F. Wilkins, *Proc. Roy. Soc. Lond.*, **1945**, *184*, 366, 390.

[40] P. Braunlich, *J. Appl. Phys.*, **1967**, *38*, 1221, 2516.

[41] J.A. Partidge, C.E. May, *J. Chem. Phys.*, **1965**, *42*, 1965.

[42] F. Aramu, V. Maxia, A. Rucci, *J.Luminescence.*, **1975**, *10*, 277.

[43] P. Braunlich, *in: Thermaluminescence of Geological Materials, Ed. D.J. McDoughall*, Academic, New York, p.61 **1968**.

[44] R. Chen, *J. Appl. Phys.*, **1969**, *40*, 570.

[45] R. Chen, *J. Mat. Sci.*, **1976**, *11*, 1521.

[46] C. Christodoulides, *J. Phys. D., Appl. Phys.*, **1985**, *18*, 1501, 1665.

[47] P. Krivits, H.J.L. Hagebeuk, *J. Luminescence*, **1977**, *15*, 1.

[48] J.M. Luthra, *Defects and Diffusion Forum*, **1989**, *62/63*, 183.

[49] K.H. Nicholas, J. Woods, J., *Brit. J. Appl. Phys.*, **1964**, *15*, 783.

[50] A. Sathyamoorthy, K.C. Bhalla, J.M. Luthra, *J. Luminescence*, **1976**, *11*, 35.

[51] R. Bindi, D. Lapraz, P. Iacconi, S. Boutayeb, *J. Phys. D., Appl. Phys.*, **1994**, *27*, 2395.

[52] W. Hoogenstraated, *Philips Res. Report*, **1958**, *13*, 515.

[53] R.K. Gartia, V.V. Ratnam, *Ind. J. Pure Appl. Phys.*, **1975**, *13*, 82.

[54] R. Chen, S.A. Winer, *J. Appl. Phys.*, **1970**, *41*, 5227.

[55] S.V. Moharil, *J. Phys. D: Appl. Phys.*, **1981**, *14*, 1677.

[56] J. Manam, *Ind. J. Phys. A*, **1994**, *68*, 105.

[57] D.R. Vij, V.K. Mathur, *Brit. J. Appl. Phys.*, **1969**, *2*, 624.

[58] I. Broser, R. Broser-Warminsky, *in: Thermoluminescence of Geological Materials, Ed. D.J.McDoughall*, Academic, New York, **1968**, p.87.

[59] D.E. Fields, P.R. Moran, *Phys. Rev. B*, **1974**, *9*, 1836.

[60] M. Boehm, P. Iacconi, K.D. Kromm, A. Scharmann, *Phys. Stat. Sol. A*, **1994**, *146*, 757.

[61] M. Castiglioni, M. Martini, G. Spinolo, A. Vedda, *Radiat. Meas.*, **1994**, *23*, 361.

3. Experimental Setup

3.1. Schematic Presentation and Description

In our laboratory we have developed a new modification of the low-temperature technique for time-correlated measurements of TSL and TSEE in cryocrystals. A schematic representation of the experimental apparatus is given in Fig. 3.1.1. Samples

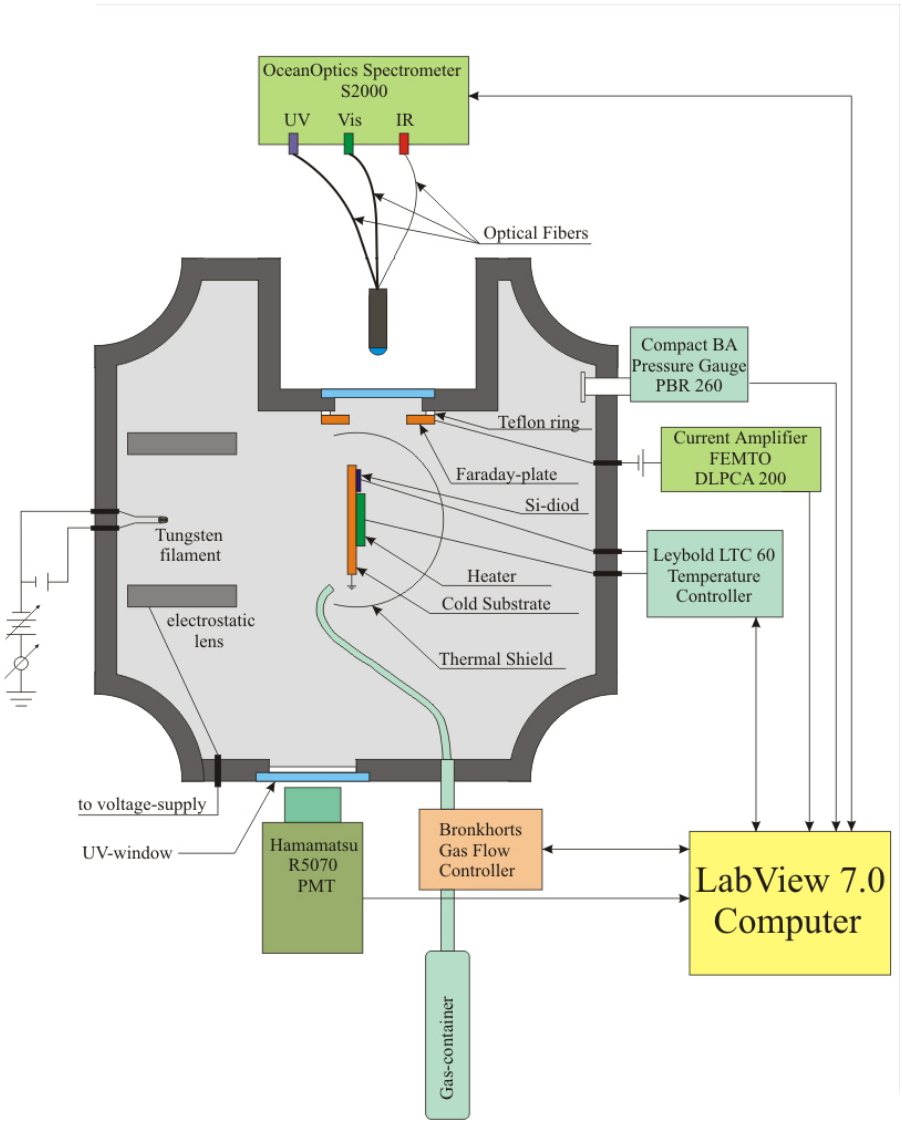

Fig. 3.1.1: A scheme of the low-temperature experimental setup for simultaneous real-time correlatated measurements of the TSEE, pressure above the sample, cryostat and substrate temperature, and spectrally resolved or spectrally non-resolved (in VUV range) TSL signals.

were prepared in a high-vacuum chamber by deposition of the gas onto a cold metal substrate. The chamber is based on ISO-K 100 standard 6-way cross with O-rings sealing. It is pumped out by 190 l/s (TPU 190) and 145 l/s (Leybold Turbovac 151) turbo-molecular pumps with DUO 1.5A and DUO 2.5 pre-pumps respectively. The basic pressure in the chamber at room temperature is about 10^{-7} $mbar$ and measured by means of a Compact BA Pressure Gauge PBR 260 provided with a digital control unit with an RS232 interface.

The substrate, Au/MgF_2-coated copper plate, is cooled down by a Leybold RGD 180 closed cycle helium cryostat (not shown in the scheme). The cryostat consists of several parts: a compressor unit, cold head and helium flex-lines. The cooling effect in such cryostats is obtained by means of helium expansion within the head module in two stages, after which helium gas returns through the low pressure line to the compressor unit.

3.1.1. Sample Preparation

Samples or gas mixtures were prepared by a standard technique in a gas handling system, consisting of two 0.5 l stainless steel containers, previously pumped out to about 10^{-6} $mbar$.

During the sample deposition, the gas flow from the gas-handling system into the vacuum chamber was controlled by a digital Bronkhorst Gas Flow Controller. The controller is connected to a computer via a serial cable. The amount of the deposited gas was established by monitoring the pressure drop in the gas-handling system.

Usually, during deposition (see Fig. 3.1.2), the samples were irradiated by a low-energy electron beam, in some experiments the irradiation occurred only after completed deposition. As a source of electrons we used a 2.2 V tungsten filament mounted in the middle of an electrostatic lens located inside the vacuum chamber about 3-4 cm away from the substrate's front surface. The energy of the electrons is determined by a potential applied to the filament and was varied only from 50 up to about 600 eV, in order to avoid "$knock-on$" defects formation. The electrons'

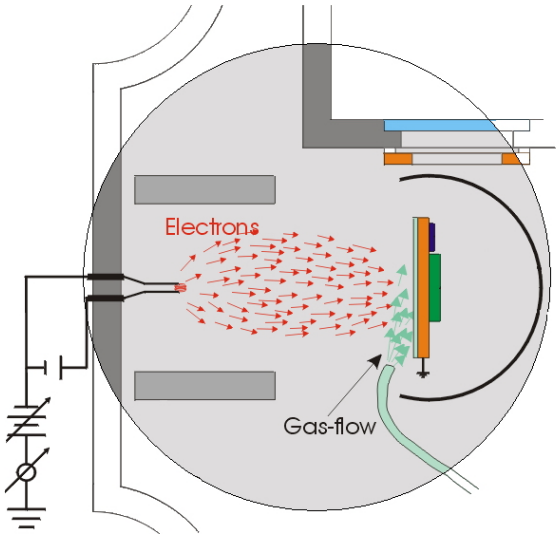

Fig. 3.1.2: Sample deposition procedure under irradiation by the electron beam.

density in the beam was usually around 30 $\mu A/cm^2$.

3.1.2. Spectrally Resolved TSL and TSEE Measurements

After the deposition was completed, the substrate rotated to one of two positions for the experimental measurements. Fig. 3.1.3 shows the substrate at the position for simultaneous TSEE and spectrally and time resolved TSL measurements. At this

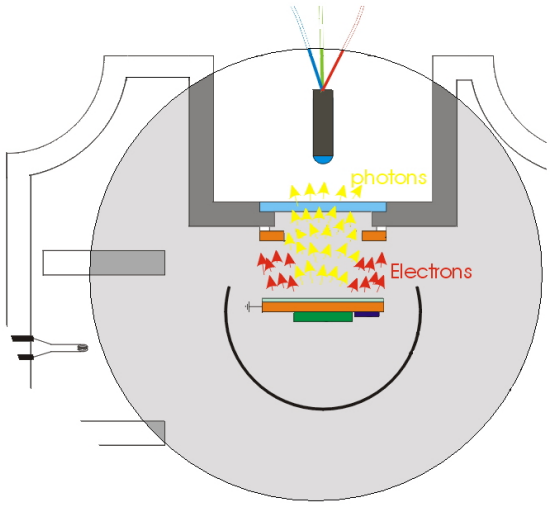

Fig. 3.1.3: The position of the substrate during TSEE and spectrally resolved TSL measurements.

position the TSEE signal is detected by a Faraday plate, Au-coated copper plate, then amplified by a FEMTO DLPCA 200 current amplifier and finally recorded by the computer. For controlling the experiment, a positive $+9\ V$ potential is usually applied to the Faraday plate in order to collect electrons more efficiently. A hole in the middle of the Faraday plate allows us to do spectrally and time-resolved TSL measurements.

The TSL spectra were recorded using a three channel OceanOptics S2000 spectrometer connected to the computer via a USB interface. The spectrometer is based on CCD detectors and allows us to record the whole spectrum in a range from 200 to 1100 nm, and integrated within a certain time-window. The minimum time is defined by the signal level and mostly varied from 3 ms to 30 s for each channel.

3.1.3. Spectrally Non-Resolved TSL and TSEE Measurements

The intrinsic luminescence of rare gas solids lies in the vacuum UV range, so that for some of the experiments it was essential to measure the TSL in that range. However, since we have no spectrometer working in that range, we used a PMT to detect the total yield of VUV photons. Fig. 3.1.4 shows the substrate rotated for simultaneous TSEE and spectrally non-resolved VUV TSL measurements. In this case the electrostatic lens is used to detect the TSEE signal. The procedure of measurement is the same as in the case of using a Faraday plate. The VUV photons are detected by means of Hamamatsu R5070 photo-multiplier tube attached to a UV window covered by a thin film of sodium salycilate ($C_7H_5NaO_3$) used as a sensitizer.

The controlled warm-up of the sample is carried out by a heater mounted to the substrate's back side. Two silicon diodes are attached to the heated substrate and used as temperature sensors. The heater and sensors are integrated to a Leybold LTC 60 digital programmable low-temperature controller. The controller connected to the computer via GPIB port is used to control the heating rate and regime. The heating parameters can be entered either by using a key-pad of the controller, or by the computer. However, in some cases entering the parameters by a key-pad is rather awkward and can easily lead to mistakes. In order to avoid these problems,

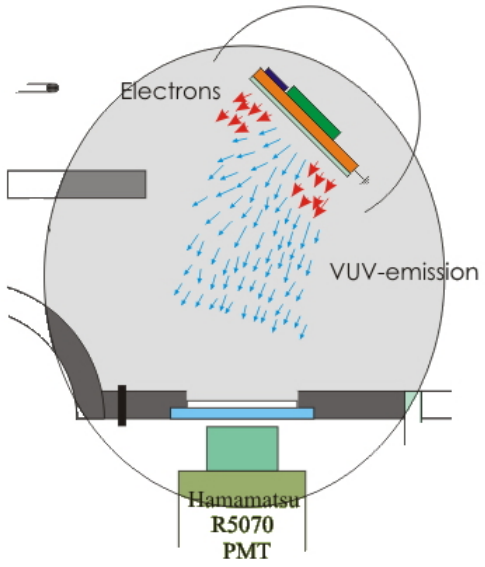

Fig. 3.1.4: The position of the substrate during TSEE and spectrally non-resolved VUV TSL measurements.

we have developed special software based on the commercial LabView7.0 program.

This software is also used for all the measurements and will be described in Appendix A. However, a few words about recording the signals have to be said. Some instruments like the pressure gauge, temperature controller, gas-flow controller, spectrometer, are provided with interfaces which can be used directly to record the signals. However, the PMT and current amplifier (TSEE) signals needed to be digitized. For this purpose we used the BNC 2110 card, which allows to convert the analog signal (voltage) to a digital one and has 16 channels, which can be used simultaneously.

While testing the program we realized that reading the temperature values from the temperature controller requires too much time, more than one second per value. To avoid this problem we decided to measure temperatures by recording the voltage changes of the temperature sensors. Using a BNC card as well as in the cases of TSEE and VUV TSL measurements, allowed us to accelerate the whole procedure of data recording. Since the BNC card allows taking the data within a few milliseconds, the time delay between two data points was limited by the time needed to transfer data from the pressure gauge, which is about 200 ms. This was

fast enough for our purpose, so that it was not necessary to further speed up the data acquisition procedure. Moreover, in order to improve the signal-to-noise ratio for TSEE, VUV TSL and temperature measurements, it was often desirable to use an integration of the signals in time. In most of our experiments the delay between two adjacent data points is around 1 s.

With this new program and modified experimental setup we are able to take simultaneously all the parameters needed to analyze TSEE and TSL on the same sample: pressure in the vacuum chamber, temperature of the sample, TSEE and TSL signals.

3.1.4. Important Notes

1. As it was mentioned above, using LTC60 temperature controller allows to control the heating rate and mode. In principle, in the experiments presented in the current dissertation only two heating modes were used: linear heating and step-wise heating. Applying the first method the temperature of the sample was changing linearly at certain a constant rate. Using the second method the temperature changed in discrete steps: first it was raised to a certain value, then it was allowed to stabilize and held constant for a certain period of time before the next temperature step. For a better understanding of this procedure one can look at Fig. 3.1.5. This picture shows temperature

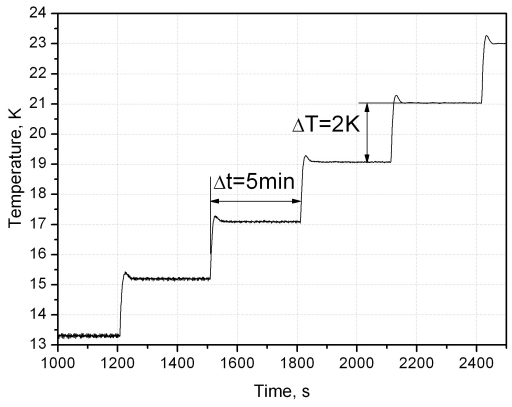

Fig. 3.1.5: The temperature changes of the sample during step-wise heating.

behavior in the case of a step-wise heating mode. ΔT defines the temperature rise for each step, while Δt defines the time between steps.

2. While testing our setup we have noticed that the temperature of the sample during preparation depends on several parameters: temperature of the depositing gas, gas-flow rate, energy of the electrons in the beam, their density and the position of the substrate. Fig. 3.1.6. shows how the temperature was changing during sample preparation. Actually, these temperature fluctuations are not high, usually within a few tenths of K. If the sample is prepared at

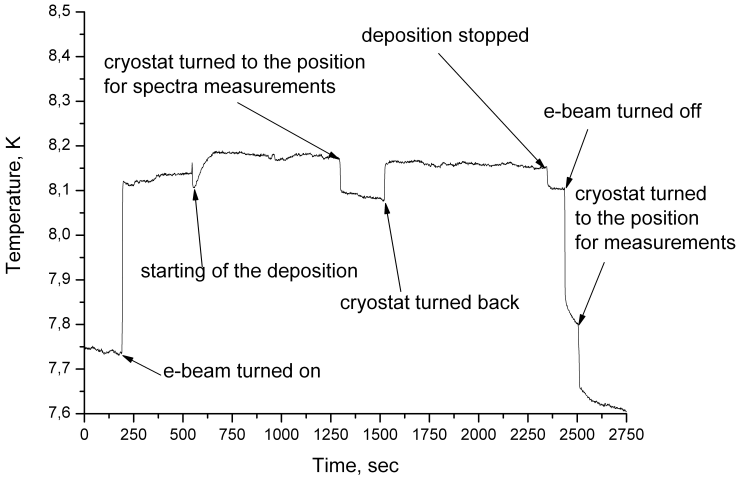

Fig. 3.1.6: The temperature changes of the substrate during sample preparation.

a low temperature, this fact may have an important effect on the structure of the sample.

3. In some cases when it was deemed necessary, the sample preparation included some additional steps. One of them was annealing the sample to a certain temperature value after deposition was completed. Sometimes, the order of the sample preparation procedures could be varied, depending on the experimental tasks. All the parameters of sample preparation for each of the experiments presented in this dissertation will be given in the corresponding sections.

4. In some instances, useful information could be gained by measuring the emis-

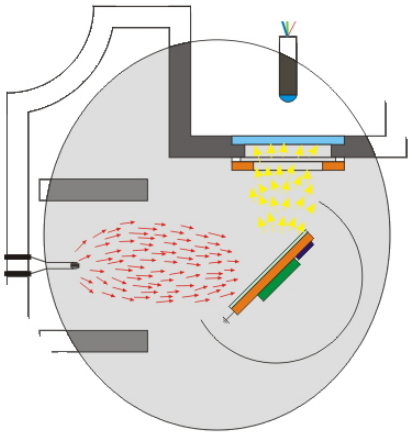

Fig. 3.1.7: The position of the substrate at which spectra can be taken during irradiation of the sample by the electron beam.

sion spectrum during sample irradiation. Such spectra give information about the electron induced processes occurring in the sample and about the ions produced by the electron impact on the sample. For such experiments the substrate was rotated to a position shown in Fig. 3.1.7.

4. Experimental Results and Discussions

4.1. Radiation Effects, Energy Storage and Its Release in Solid Rare Gases

4.1.1. Introduction

When a solid material is exposed to high-energy radiation - VUV photons, electrons, or ions, a "*damage*" of the solid occurs, with part of the excitation energy remaining stored in the crystal. The defects may include vacancies, interstitial or impurity atoms, radicals, ionic centers, and trapped electrons. From the technological point of view, such damage results in changes in the properties of the solid, and may for instance adversely affect material strength. Conversely, in other situations, one may use an intentionally introduced damage centers to optimize the material properties for a desired application, e.g. F-centers or implanted ions for solid state lasers, or dopants in semiconductor manufacture.

Condensed rare gases are very simple, theoretically tractable solids, and the damage produced by irradiation was extensively investigated [1–9] with the most common defects following a moderately high energy irradiation being the so called intrinsic ionic centers. The radiation ionizes atoms of the solid, and, unless an immediate recombination with the electron takes place, the Rg^+ ions will promptly react with one of the neighbor atoms to form strongly bound, compact Rg_2^+ ionic centers. Since overall the solid has to remain approximately neutral, a comparable number of electrons must also be present, but less is known about their exact whereabouts. Most are probably trapped at various defect sites, grain boundaries or attached to impurities. Once the Rg_2^+ ions are formed, a Franck-Condon barrier will hinder their neutralization, and the ionic centers will be effectively "$self-trapped$".

The amount of energy stored in the solid during the sample irradiation may be quite appreciable, and when the sample is then allowed to gradually warm up, various processes can be "*activated*", with a part of this stored energy being released. The electrons may be promoted from shallow traps into the conduction band, and then neutralize positively charged ions. At higher temperatures also atoms and impurities may start to diffuse through the solid and react, and the energy released in these processes can be manifested in various ways. The methods based on the observation and monitoring of the resulting effects are often referred to as "*activation spectroscopy*", and they provide useful information and insights into the nature of the defects, and about the processes proceeding in the sample. In the most common type of such experiment, one simply monitors the intensity of the "*Thermally Stimulated Luminescence*" or TSL as a function of temperature, to obtain the so-called "*glow curve*" [10]. TSL from "*pure*" rare-gas solids was studied in several publications - after irradiation with X-rays [11, 12], synchrotron radiation [9–13] or electron beams [14–18]. A more detailed information than from simply recording the glow curve can of course be obtained by spectrally resolving the TSL.

In the case of "*pure*" rare-gas solids, the strongest luminescence observed is the well known "$M-band$" located in the VUV range, which results from an electron - self-trapped hole neutralization. This band which is quite broad is due to the $^{1,3}\Sigma_u^+ \rightarrow {}^1\Sigma_g^+$ bound-free transition of the neutral rare gas dimers, Ar_2^*. The primary step in the neutralization reaction is presumably a promotion of one of the trapped electron into the conduction band of the solid, and as our previous studies have shown, besides neutralizing an existing trapped "*hole*", such conduction band electrons can also be directly extracted from the surface of the sample, and detected as a "$Thermally\ Stimulated\ Exo-electron\ Emission$", or TSEE [16–20]. Finally, our previous studies suggested that the excess energy set free in the neutralization process can be transferred through the solid, and result in an anomalous, low temperature ejection of surface atoms from pre-irradiated samples. By simultaneously monitoring all three effects, the TSL, TSEE and the surface atom ejection - mani-

fested by a pressure rise - one can get a more detailed "$fingerprint$" of the sample damage, and a better understanding of the types and nature of processes occurring in the sample, than with a study of the TSL alone.

In the most common version of TSL experiments the samples are linearly heated, which has the drawback that the temperature, the defect concentrations and the rates of various processes are all changing simultaneously. The observed data then also depend on the rate of temperature change, which makes the interpretation of the results more difficult. A useful alternative to linear heating, used in this study, is to raise the temperature in a series of discrete steps, monitoring the time evolution of the luminescence and other observable quantities after each step at a constant temperature.

In view of the sensitive dependence of the TSEE, TSL and other phenomena upon the sample structure, impurity concentration, and other variables, it is obviously preferable to perform a time correlated measurements of all the thermally stimulated phenomena simultaneously, on the same sample to get reliable results and come to solid conclusions. For this purpose we have recently constructed a new apparatus specifically designed for such activation spectroscopy studies, which allows us to monitor and record the TSEE and TSL as well as pressure in the cryostat chamber - as an indicator of the surface atom desorption - in a single experiment. The new apparatus includes a digital temperature controller which makes it possible to program arbitrarily the temperature rise.

In the present manuscript we apply this new setup to the investigation of simple, nominally pure rare gas solids - mainly argon in this paper - after they were exposed to an intense electron beam radiation by the activation methods. We gain additional useful insights by comparing measurements obtained with linear heating, with experiments where the temperature is raised in a series of discrete steps.

4.1.2. Experimental Details

The experiments described in this chapter were carried out on the apparatus mentioned in the previous section. The solid rare gas samples were grown on the sub-

strate kept at 7 K. The base pressure of the vacuum chamber was about 10^{-8} $mbar$. A high-purity (99.999%) Ar gas was used. The deposition rate was $10^{-1}\mu ms^{-1}$. Final sample thicknesses were around 50-100 μm. To generate charge centers throughout the sample volume, the electron beam was usually on while the sample was being deposited. However, in some experiments the irradiation took place after the completed deposition. As a source of electrons a 2.2 V tungsten filament was used, the electron energy could vary from 100 to 500 eV with the current density being kept at 30 μAcm^{-2}. After the sample preparation was completed, the substrate was rotated to the position for correlated TSEE and spectrally non-resolved VUV TSL measurements.

4.1.3. Results and discussions

Linear Heating of pre-irradiated solid Ar The results of a typical "*correlated activation spectroscopy*" experiment, using the conventional linear sample heating, are presented by dashed lines in the Fig. 4.1.1. In this experiment, argon gas was deposited over 30 min (flow 2 STP ml/min) on a cold 7 K substrate, with a simultaneous sample irradiation by 500 eV electrons. After the completed deposition, the sample temperature was linearly raised to above 45 K, at a rate of 3.2 K/min, while monitoring the intensity of the VUV luminescence, to obtain the "*glow curve*" of intensity versus temperature in Fig. 4.1.1 *a*.

It should be noted, that even though the rare gases used were nominally pure, one invariably observed, besides the intrinsic luminescence due to the rare gas itself, also emissions due to impurities. Since our experiments are carried out in a conventional, matrix isolation setup with a base pressure around 10^{-8} $mbar$, these can not be completely avoided. In particular, the green, long-lived, doubly forbidden ^{2}D$\rightarrow^4$S phosphorescence due to N atoms is invariably observable, as well as O atom line, ^{1}S$\rightarrow^1$D transition, and very weak molecular emissions. These all occur in the visible and near UV ranges, are well known and relatively weak. They do not interfere with the experiment, so they will not be further discussed here.

As already noted, the most abundant defects generated in the rare gas solids

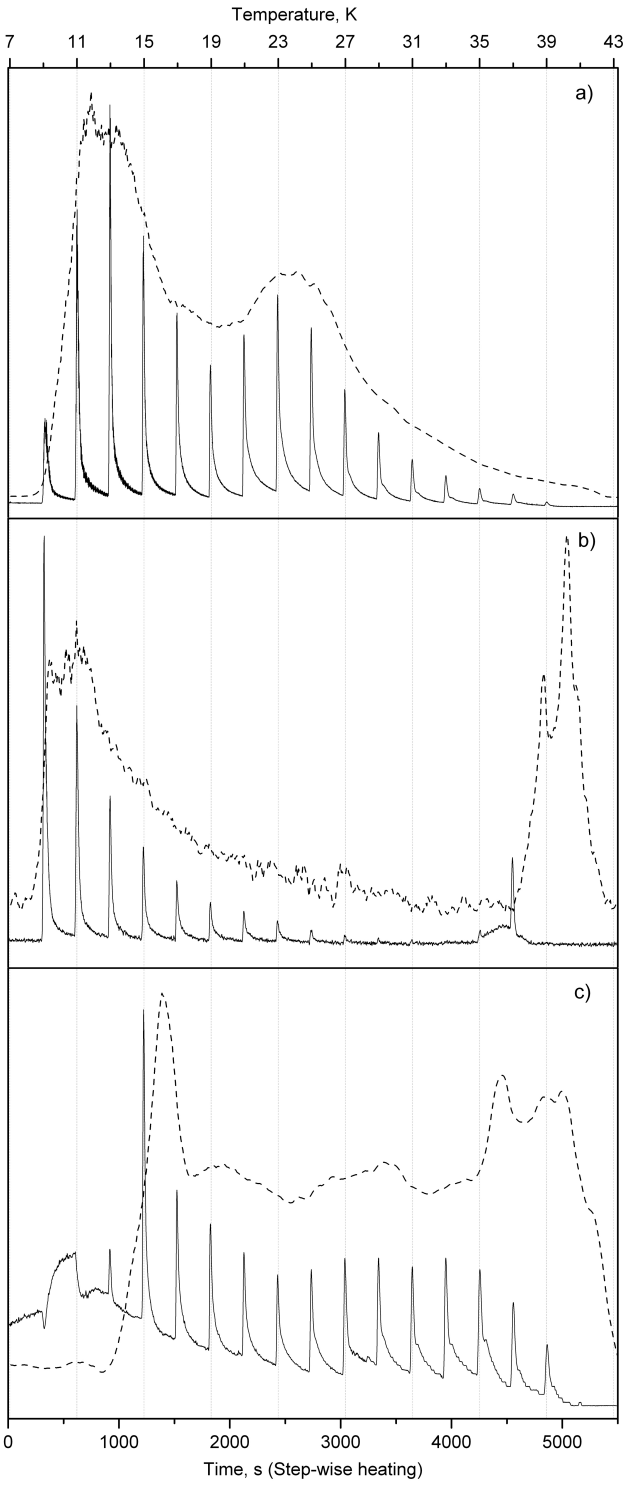

Fig. 4.1.1: Comparison of the results of the linear heating (dashed lines) and stepwise heating (solid lines) experiment data. (a) - The TSL VUV emission, (b) - TSEE current and (c) - pressure in the chamber and its rise due to anomalous surface atom desorption.

during the irradiation are the self-trapped ionic Rg_2^+ centers, and the trapped electrons. As already noted, as the sample temperature is raised, promotion of the electrons into the conduction band allows them to move around, and neutralize the positive ‘‘*holes*″, resulting in the “$M-band$″ VUV photon emission. The typical “*glow curve*″ - the dashed line in Fig. 4.1.1 *a* - is obtained by monitoring this VUV “*pure*″ rare gas TSL, by far the strongest emission observed. One can see, that the luminescence intensity starts to rise abruptly around 9 K, reaching a rather flat maximum between about 11-14 K. It then goes through a minimum between 17-21 K, before rising again, and displaying a second broad maximum centered around 23-25 K. Finally it gradually decays to essentially zero around 41 K, corresponding to a complete, final loss of the sample. The appreciable “*noise*″ observable on the first, lower temperature, peak is actually due to small temperature fluctuations associated with the movement of the displacer of the closed cycle refrigerator used in the experiment. The two broad maxima might appear to suggest that the electrons are located in two different “*sites*″, with different activation energies.

As also noted above, some of the electrons promoted into the conduction band can be extracted from the sample and detected as TSEE current, as shown in the trace 4.1.1 *b*. Like the TSL, also the current appears slightly below 9 K and rises sharply to a broad, structured maximum between 9 and 12 K. Interestingly, though, there is no indication of a second maximum around 24 K, but unlike the TSL, the TSEE curve decays gradually to essentially zero above 30 K. The second, strong and rather sharp maximum between 37 and 41 K, is presumably due to electrons and negative charges in traps too deep to be thermally promoted to the conduction band, which are, however, released when the sample evaporates and its integrity is lost.

During the experiment, we have also continuously monitored the pressure in the cryostat chamber, with the results displayed in the Fig. 4.1.1 *c*. The base pressure in our cryostat is typically around 10^{-8} $mbar$ at the about 7 K base temperature, but it increases somewhat during sample preparation, being a few times 10^{-8} $mbar$ just after the deposition is stopped. As one can see in the figure, during the heating

process the pressure first remains relatively constant but starts to rise sharply around 13 K, reaching near 16 K a maximum high above the base pressure, even though the vapor pressure of argon at this temperature should be negligibly small. Above 17 K the pressure drops again but remains elevated well above the base pressure, fluctuating slightly. The second, poorly defined and structured maximum around 35-42 K is again close to the range where the solid starts to lose its integrity. The pressure then drops sharply and approaching the base value in the low 10^{-8} $mbar$ range signaling the sample evaporation and loss.

Stepwise Heating Experiments To gain a better understanding of the processes taking place in the solid, we have repeated an experiment described, this time programming the controller to increase the temperature not linearly, but in a series discrete 2 K in five minute intervals. To permit a better comparison with the continuous heating, the results of such experiment are included in the Fig. 4.1.1. The stepwise heating experiment, shown here by solid lines, was carried out, except for the different, stepwise heating regime, carried out under essentially identical conditions as the experiment discussed in an earlier section, and represented by the dashed lines. In the stepwise experiment, after each 2 K increase the temperature stabilizes at the new value in less than about 20 s, and is then held constant - for 5 min in the experiment shown. As can be seen in the Fig. 4.1.1, all the three observed effects mentioned above, the TSL, TSEE and pressure exhibit very similar behaviors, with the signal rising sharply after each temperature step, and then, while the temperature is held at a constant value, decaying to essentially zero before the next temperature step. In the TSL VUV luminescence in Fig. 4.1.1 a the first step occurs at 9 K, and while the heights of the individual peaks are different, it is easy to see but that the intensity envelope follows rather closely the intensity distribution found in the linear heating "*glow curve*". Similarly behaves also the TSEE, the exoelectron current as shown in the Fig. 4.1.1 b, as well as the chamber pressure in the vacuum chamber in Fig. 4.1.1 c. In each case, the temperature step results in a sharp rise in the signal, followed by its gradual decay to almost zero, and in each

case the envelopes of the peak heights in the stepwise experiments roughly follows the intensity distribution in the linear heating experiment given by the dashed lines.

While the envelopes of the stepwise heating peaks behaves for each of the effects investigated similarly to the continuous heating experiment, however, the comparison of signal intensity distributions for the three different effects shows that there are significant differences. For instance, in the case of TSL the first, 9 K peak is relatively weak, and increases to a maximum at 13 K, but for TSEE is the 9 K signal actually by far the strongest, and the peak intensities then steadily decline, to become, on the scale of the figure, nearly unobservable above 30 K. Note, that like in the linear heating experiment, there is not hint of a second peak near 25 K, which is apparent in the TSL experiments. Near the range where the integrity of the sample is lost the TSEE current reappears, with clear maxima at 35 and 37 K. The chamber pressure above the sample exhibits the first clear rise at the 13 K step, with by far the most intense peak occurring at 15 K, close to the temperature where the sharp pressure maximum is found in the linear heating experiment. At higher temperatures a clear pressure rise is observed at each step, essentially up to the temperature where the sample is lost. As already noted above, most of these anomalous pressure peaks occur at temperatures deep below the conventional sublimation point of the solid, where the equilibrium argon pressure should be negligibly small and unobservable.

Signal Rise and Decay in the Stepwise Heating Experiment Also a more detailed comparison of the three effects investigated, TSL, TSEE, and pressure, reveals additional similarities in their behavior. Beyond the fact that for each of the effects a sharp signal rise accompanies each temperature increment, also closer analysis of the shape of individual peaks in the stepwise experiment confirms their parallel behavior, as exemplified by the 15 K temperature step in Fig. 4.1.2. The peaks for all three effects show similar fast rise-times, followed by a gradual decay. While at a first sight the signal decay after each step might appear exponential, actual numerical least square fitting yields rather poor single exponential fits, as shown in the panel Fig. 4.1.2 a (dotted line). Most of the decays can, however, be almost

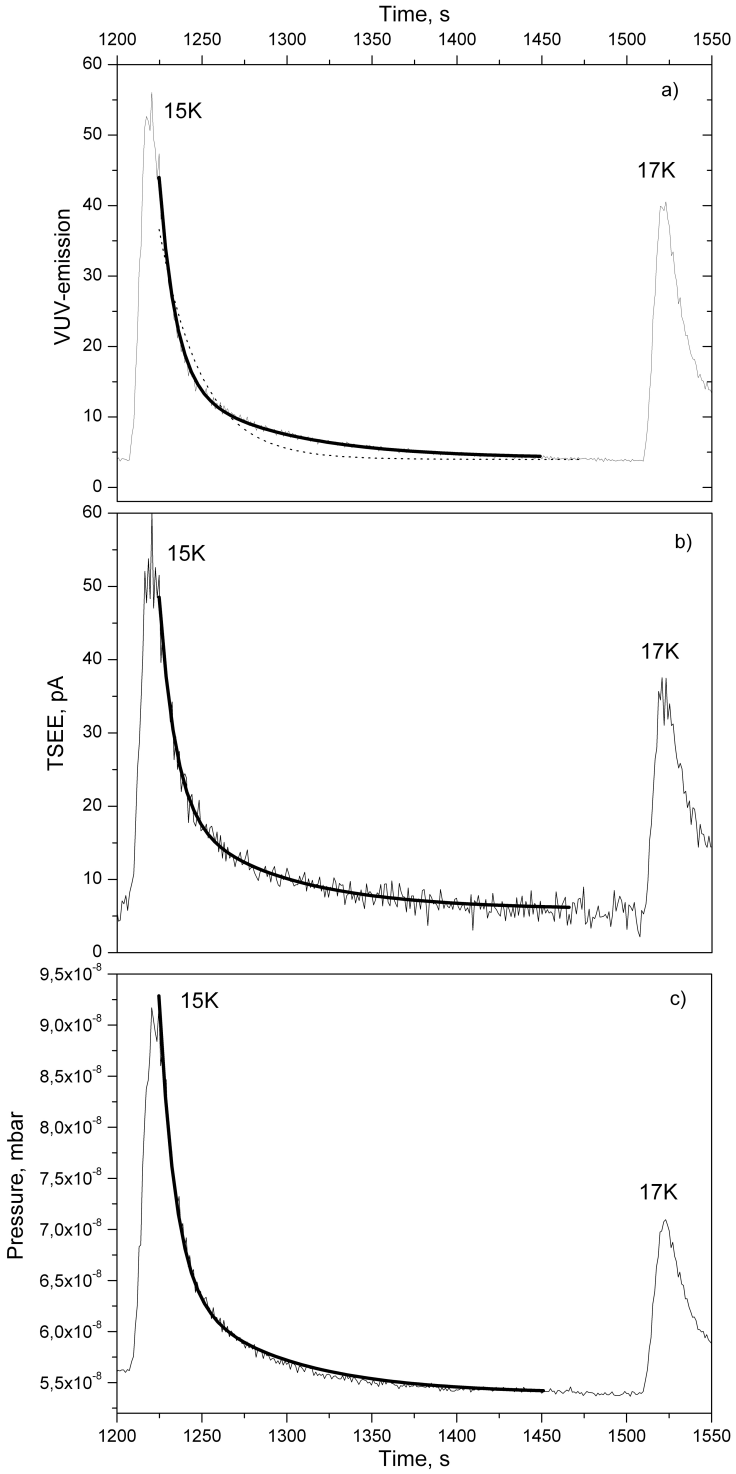

Fig. 4.1.2: Least square fitting of the decay of the TSL (a), TSEE (b)and pressure signals (c), appearing after temperature was increased in a 2 K step (from 15 K to 17 K). The single exponential (thin dashed line in panel (a) gives a poor fit, but the almost perfect double exponential fits of the data (heavier solid line).

perfectly fitted by double exponentials (solid heavier line). If one tries, at a given temperature, to fit the decay of the TSL, TSEE and pressure data separately, the lifetimes - or decay constants - one obtains for the three processes differ slightly, but this is mainly due to the fact in multi-exponential fits the values of exponents are usually strongly correlated. As demonstrated in the panels Fig. 4.1.2 *a*, *b*, and *c*, all three decays can be extremely well fitted by the same set of two lifetimes, in this specific case 9.75 and 52.4 *s* with, however, the ratios of the two pre-exponentials being slightly different, i.e. in the example shown 2.3, 2.2 and 1.7 for the TSL, TSEE, and pressure signals, respectively.

Comparing the fitted lifetimes at various temperature steps, one finds that the first, shorter lifetime does not vary appreciably, and is in most cases within the experimental error almost identical - between 8-12 *s*. Obviously, as confirmed by examination of the experimentally measured temperature curve of the substrate, the "*steps*" are not really instantaneous, but about 25-30 *s* are always needed for the temperature to rise the 2 *K* and stabilize. The first, fast decay exponential is therefore not really occurring at a constant temperature, but during the time the temperature is changing, and the 8-12 *s* decay obtained in the fit can only be viewed as an upper limit for the rate of the process responsible for the signal rise. The second, longer exponentials are considerably slower, with fitted lifetimes in the range of 80-120 *s*, and with the signal decay persisting well after the temperature was stabilized at the new value.

The Processes Occurring During the Sample Warm-Up Perhaps the most important aspect of the stepwise heating experiment lies in the observations of an almost perfectly parallel behavior of the three measured effects. This parallel behavior, including the within the experimental error identical lifetimes - or rate constants - deduced from the data show beyond reasonable doubt, that the three processes are intimately linked together. In trying to understand these observations, one can first recall that, as noted above, the main effect of the high energy electron irradiation will be the generation of a distribution of intrinsic self-trapped holes in the solid,

Ar_2^+ in the case of pure argon. Obviously, since overall the sample must remain nearly neutral, a comparable concentration of negative species, mainly trapped electrons in the present case, must be present. The detrapping of these electrons from shallow traps due to the temperature increase is then undoubtedly the primary process, which leads to all three of the observed dominant effects discussed above, VUV TSL, TSEE, and the anomalous pressure rise (discounting again the weak visible and near UV impurity emissions).

When a detrapped electron neutralizes one of the ionic Rg_2^+ dimers, a highly excited neutral dimer Rg_2^* is formed which may then partially relax by a rapid, complex nonradiative cascade, and will eventually return to the ground electronic state, in most cases by emitting a photon. The energies of these photons are in the VUV range, and they are detected as the VUV TSL discussed above. In a competing process, if the detrapped electron is located close to the sample surface, it may, rather then recombining with an Rg_2^+ cation, be extracted by an applied potential and accelerated to the detector, where it is monitored as the TSEE current.

As noted above, the equilibrium distance between two neutral rare gas lattice atoms is nearly twice as large as the bond length of the positively charged Rg_2^+ ion (or of a highly excited Rg_2^* Rydberg state). The vertical radiative TSL transition will therefore terminate high on the repulsive limb of the ground state dimer potential:

$$Ar_2^+ + e^- \rightarrow Ar_2^* \rightarrow Ar + Ar + \Delta E + h\nu(VUV) \quad (4.1.1)$$

As the ground state molecule then nonradiatively relaxes towards the potential minimum, the considerable excess - potential - energy is converted into kinetic energy of the two atoms, which in turn will strike atoms of the surrounding rare-gas "*cage*". An interesting effect can then occur, with the kinetic energy of the dissociating Ar_2 dimer atoms not being dissipated in a conventional, thermal diffusion fashion, but propagating away from the relaxing molecule as a ballistic "*soliton*" wave [21, 22]. The energy is in this way efficiently and resonantly transferred through a row of closely packed lattice atoms, in an effect analogous, in the macroscopic world, to that observed in a toy, often referred to as "*Newton's Cradle*",

and also well known to any pool player. When the first one of a row of identical balls in contact is struck, the kinetic energy propagates efficiently and with little loss through the entire row, and is imparted to the last one. In the solid rare gas it may propagate through the row of lattice atoms, and if or when it reaches the crystal surface, it may dislodge one of the atoms, and result in the anomalous atom desorption or evaporation.

The nearly perfect correlation between the TSL photon emission and the pressure rise we observe establishes the intimate connection between the two processes beyond any doubt, and proves that the self-trapped hole neutralization during controlled annealing of pre-irradiated rare gas solids does indeed lead to the anomalous, low temperature surface atom desorption [23, 24]. This evaporation of a substantial number of atoms which accompanies electron-hole neutralization according to Eq. (4.1.1), also confirms the results of recent molecular dynamics studies [21], which concluded that energy can in this way be efficiently transferred over distances exceeding hundreds of lattice constants.

Effects of irradiation time, sample thickness, and electron energies To examine dependence of the degree of sample damage upon irradiation time, a series of identical samples was, after a completed deposition, exposed the 500 eV electron beam for times ranging from 1 to about 60 min, with the Fig. 4.1.3 showing the behavior of integrated current, and integrated TSL as a function of irradiation time.

The results reveal that the TSL intensity while initially growing approximately linearly with the irradiation time, quickly starts to saturate and level off. Thus increasing the time from 10 to 60 min results in only about a 60% increase in the signal, and a similar saturation and behavior was observed also for the pressure rise. Interestingly, the TSEE saturated even much faster, and beyond about 40 min the current actually started to decrease with extended irradiation. This probably reflects the fact, that electrons can only be extracted from a relatively thin surface layer. Once this layer is saturated with the charged species, additional irradiation is apparently comparably efficient in destroying the existing ionic species as it is in

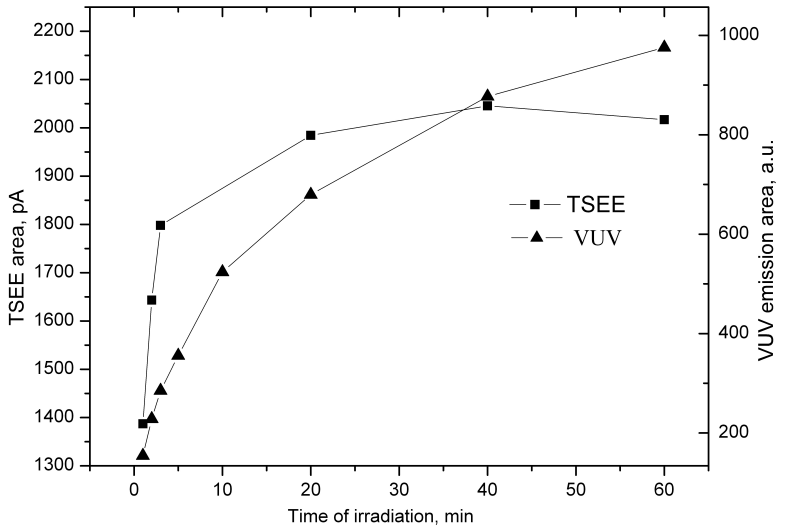

Fig. 4.1.3: Dependence of the integrated TSEE current and of the TSL VUV emission of samples, irradiated after deposition by 500 eV, upon the length of the irradiation time

forming new ones, so that TSEE signal does not further increase. This explanation is confirmed by similar experiments, where layers of various thicknesses were grown with a simultaneous irradiation. While the TSL signal increased approximately linearly with time and thus the amount of sample deposited, there was no observable increase in the TSEE signal beyond about 10 min deposition, which corresponded to a sample thickness of just a few μm. Apparently, the contribution of electrons deeper in the sample to the observed TSEE is insignificant. This is also in agreement with the results [26] where an electron escape depth of about 500 nm was found.

We have also examined the effect of the electron energies by irradiating otherwise identical samples (about 10 $mmol$ deposited over 30 min with 100, 200, 300 and 500 eV electrons (Fig. 4.1.4). The VUV TSL intensity (Fig. 4.1.4 a) was actually increasing faster than linearly, growing more then ten-fold upon raising the beam energy by a factor of five from 100 to 500 eV. Also the shape of the "$glow\ curve$" changed somewhat, and while the 12 and 24 K maxima were nearly identical in the 100 eV experiment, at the higher electron energies the distribution shifted in favor of the lower temperature, 12 K maximum.

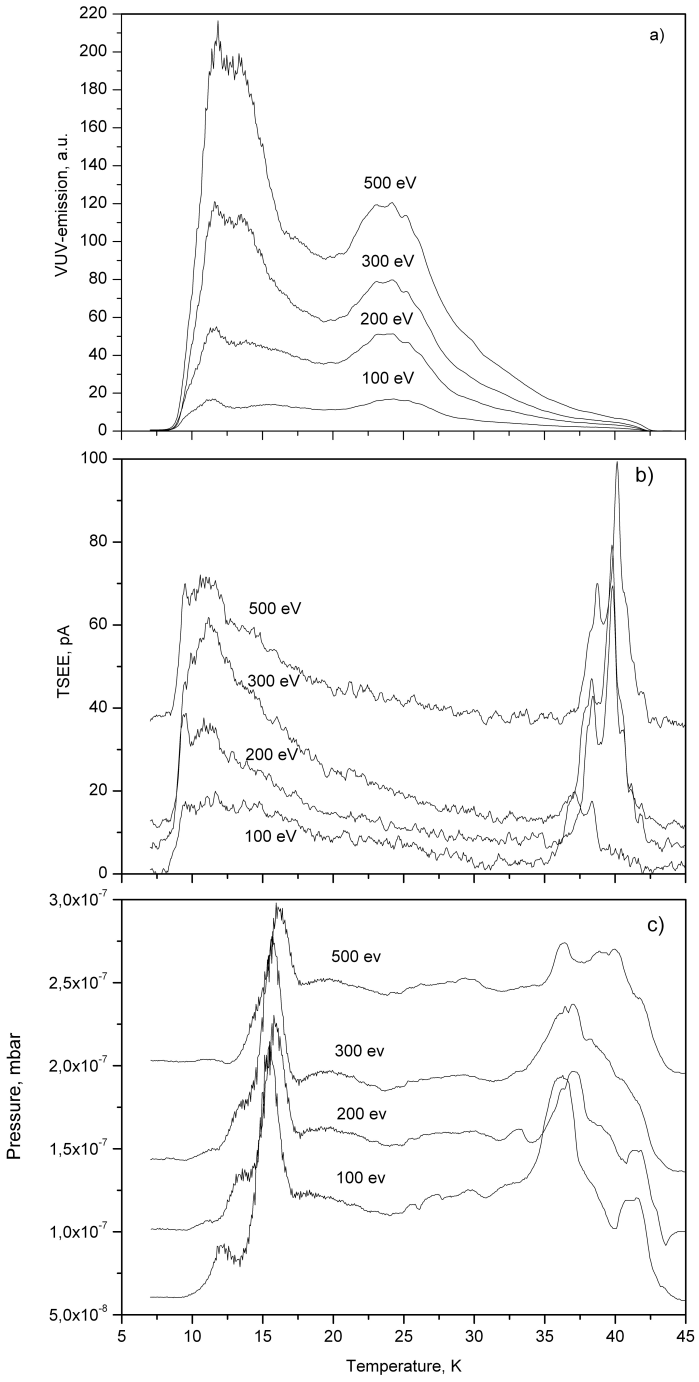

Fig. 4.1.4: The VUV emission curves (a), TSEE curves (b) and pressure rises in the vacuum chamber (c) from the samples irradiated after deposition by electrons with different energies

As might be expected, in contrast with the TSL intensity, the increase in the TSEE electron current was much less dramatic (Fig. 4.1.4 *b*), doubling approximately between 100 and 300 eV, and exhibiting essentially no further growth in the 500 eV experiments. This can again be understood if one realizes that the extracted electrons come mainly from the thin subsurface layer. The 100 eV electrons possess large ionization cross-sections, and they will undoubtedly preferably ionize atoms near the surface, generating less hole-electron pairs deep in the sample. This effect becomes even more important if one considers that the irradiation can produce in the sample a small negative space charge, which will even further slow down the incoming electrons.

The 500 eV electrons, on the other hand, can surely penetrate much deeper into the sample, and furthermore a single electron has undoubtedly enough energy to ionize several argon atoms throughout the sample volume. Again, ion pairs produced deeper in the sample while enhancing the TSL, will contribute little to the TSEE current, which is preferentially extracted from the subsurface layer. Interestingly, the largest pressure rise during the sample heating was observed in the 100 eV experiment (Fig. 4.1.4 *c*), and in fact decreased slightly at higher electron energies, being about a factor of two lower at 500 eV.

Repeated Sample Irradiation, and Ion-Center Regeneration Obviously, if the sample temperature is increased much above 40 K the sample evaporates and is irretrievably lost. If, however, the controlled heating is stopped below the sample loss temperature and recooled, then it should be possible to regenerate the ions lost in the annealing process by a repeated irradiation with the electron beam. In several series of such experiments we have stopped the controlled annealing at a temperature well below where the sample loss occurs, and irradiated the sample again after recooling it to the 7 K base value with the data summarized in a three-dimensional form in the Fig. 4.1.5. The argon sample was first deposited at 7 K without irradiation, subsequently irradiated, then heated up to 27 K - at which point some 80% of the ionic species have recombined - and then re-cooled back to

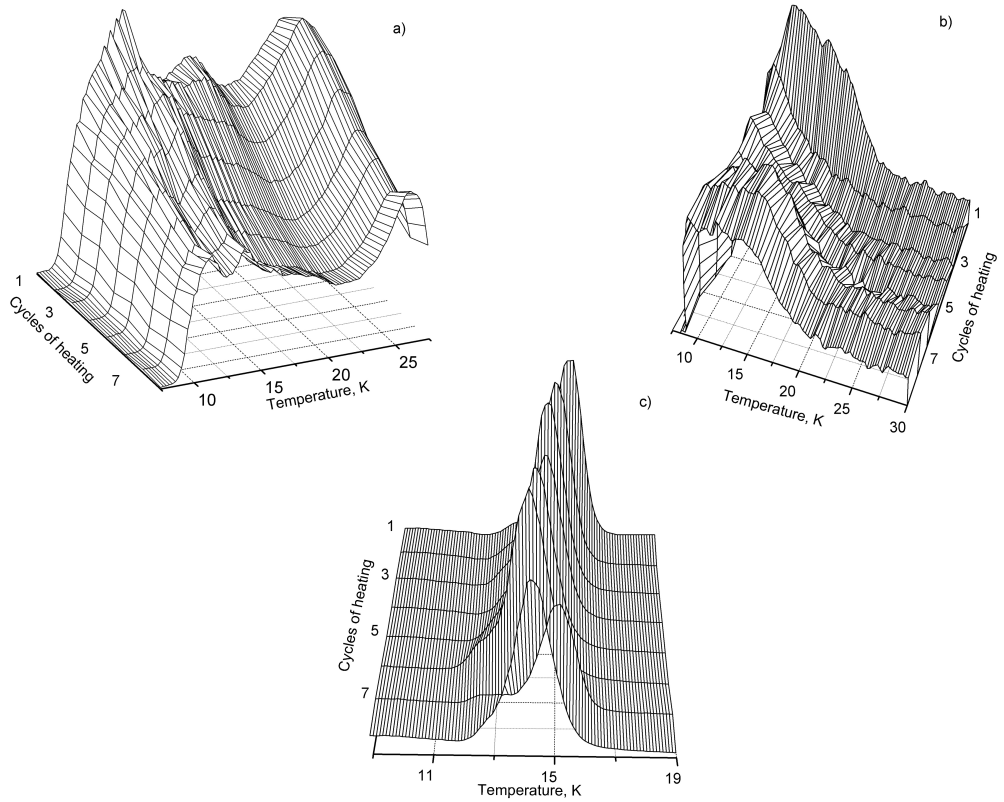

Fig. 4.1.5: Three-dimensional presentation of the results of an experiment, where a layer of solid argon was deposited, without photolysis, for 30 min, and subsequently subjected to the cycle: (irradiate 30 min by 500 eV electrons - anneal to 27 K while monitoring the TSL, TSEE and pressure - re-cool to 7 K) repeating it eight times. After irradiation of 7^{th} cycle a thin layer of non-irradiated Ar on top of the sample was deposited. Trace (a) - VUV TSL, (b) - TSEE, (c) - pressure in the cryostat.

7 K. Subsequently this cycle: (- irradiation by electrons for 30 min; - heating to 27 K while recording the TSL, TSEE and pressure signals; recooling then back to 7 K) was repeated up to eight times. The data in Fig. 4.1.5 clearly show that during each cycle new energy is deposited in the solid, with its release upon heating always resulting in a strong TSL, TSEE, and in the anomalous pressure rise.

In the Fig. 4.1.5 a one can see, that during the first few cycles the intensity distribution in the TSL glow curve changes slightly, with the lower of the two intensity peaks (which appear at 12 and 24 K in the first cycle) splitting into two maxima at 10.5 and 13 K, and also the integrated TSL signal intensity decreasing slightly. After about 4-5 cycles, however, these changes stop, and in later repetitions the

TSL stays almost perfectly reproducible from cycle to cycle. Similar is the TSEE situation shown in Fig. 4.1.5 *b*, where the current maximum located near 9-10 K in the early cycles broadens somewhat in the later cycles, extending from 10-15 K, and becomes again essentially constant after 4-5 cycles.

Also the anomalous pressure rise repeatedly appears after each irradiation cycle (see Fig. 4.1.5 *c*) but the results are somewhat puzzling. The sharp maximum which is centered around 14.2 K in the second cycle, shifts during the following cycles progressively to slightly lower temperatures, so that in the later cycles of this experiment, (n=5, 6) it is located near 12.9 K, clearly downshifted from the first cycle. After completing the 7^{th} cycle irradiation we have in this experiment deposited a very thin layer of non-irradiated argon on top of the sample, before recording of the annealing data. While this thin layer had almost no effect upon the TSL or TSEE curves, it resulted in a much lower pressure rise and in a shift of the maximum almost back to its position in the 1^{st} cycle, at 14.2 K. In the subsequent, 8^{th} cycle, however, (now carried out again without any additional deposition), the peak shifted back, coinciding with the 6^{th} cycle maximum. We will defer our discussion and tentative interpretation of some of these observations until somewhat later.

Effect of Sample Annealing One can also get a better understanding of the linear heating experiments and in particular the slight but clearly discernible changes from cycle to cycle in the repeated photolysis - annealing experiment. At least part of these changes is due to sample annealing. While in the early cycles, right after the sample deposition, the solid surely contains a number of structural defects, such as vacancies, interstitials or displaced atoms, or grain boundaries, these will upon repeated cycles be partially removed by the annealing process, resulting in more perfect, crystalline layers. We believe that the gradual shifts in the pressure peak in the experiment exemplified in the Fig. 4.1.5 *c* to lower temperatures may be the result of an improving thermal conductivity of the more perfect, annealed crystals. In the early cycles there will be a steeper temperature gradient and a larger lag between the temperature of the substrate, and that of the sample surface.

This lag will be progressively decreasing with the repeated sample annealing. With this in mind, one can also understand the "*anomalous*" behavior in the 7^{th} cycle: the kinetic energy resulting from neutralization of the Ar_2^+ dimers had here to be transferred through the thin unannealed and unphotolyzed argon layer. This shift is then reversed, after the top layer has been photolyzed and annealed during the 8^{th} cycle.

Trapped Ion Energies and "Coulombic Landscape" The results showing that each little temperature step gives a steep increase in the measured signals would suggest that there are not just two distinct "*sites*", and traps with two different depths - as might seem to be implied by the two maxima observed in the glow curve of the continuous heating experiment. Rather, the stepwise experiments suggest an almost continuous distribution of sites and electron traps with different depths, so that each small temperature increase makes additional electrons accessible for thermal detrapping. At first thought one might ask how can there be, in the "*simplest of them all*" rare gas solid lattice, so many distinct sites. More commonly one finds in rare gas matrices for atoms or simple molecules just a few - frequently two - well defined distinct sites, which are often attributed to the presence of *hcp* and fcc local environments.

There are, however, important differences between neutral and charged species. The neutral guests interact with matrix atoms by the very short range dispersion or repulsion forces, and their energy will in principle only be affected by the nearest neighbor atoms. Electrons and ionic species, on the other hand, are subject to electrostatic, Coulombic interactions, which are, even when screened by the solid matrix, relatively long range. Thus in matrices containing a random distribution of positive and negative ions, the energies of the individual trapping sites will be modulated by these Coulombic attractions and repulsions due to nearby ions or electrons. This may result in an almost continuous distribution of "*traps*", with different energies needed for detrapping of the electrons. It might also be worth mentioning that, if the Coulombic interactions are considered, the depths of the electron traps

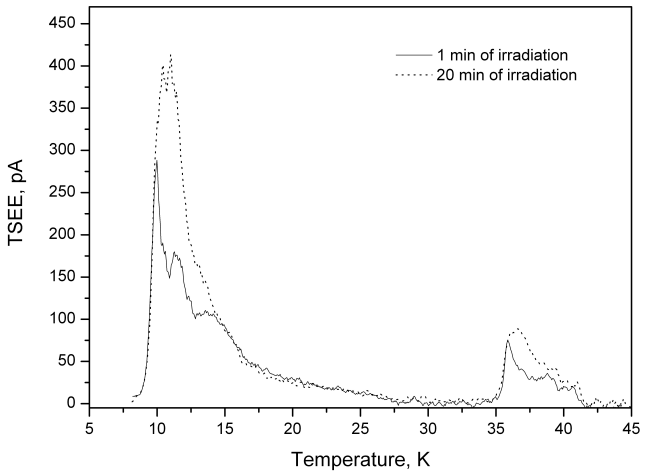

Fig. 4.1.6: Comparison of the TSEE curves of solid Ar samples pre-irradiated by 500 eV electrons for 1 min and 20 min, respectively.

are not constant, but will change continuously during the experiment. Each time some charged species - holes, electrons or other ions - in the neighborhood of a given trapped electron are lost due to their detrapping, neutralization, or to their being extracted from the sample, the "$Coulombic\ landscape$" will also change, and so will the depth of the trap in which it is located.

These changes in the activation energies needed for electron detrapping based upon the content of ionic species is evidenced by subtle changes in the TSEE curve shapes depending on irradiation dose. As can be seen in the Fig. 4.1.6, the hints of fine structure which are present in the TSEE curve at short irradiation time are lost after longer irradiation and the peaks broaden appreciably. In connection with the free electrons trapped in solid Ar (or Ne) it should perhaps also be noted, that it actually requires energy to introduce an electron from vacuum into the perfect solid lattice. In other words, the perfect solid has a negative electron affinity (about -0.4 eV in the case of argon [25]), so that the electrons are trapped at "$defects$" such as vacancies, dislocations, grain boundaries or at impurities with positive electron affinities or, very likely, partially stabilized by Coulombic interactions mentioned above due to nearby ionic species.

Understanding the nature of processes resulting in the observed effects, one

can now immediately speculate that, for instance, the differences in the overall intensity distribution of the TSL and TSEE curves shown in the Fig. 4.1.1 are at least partially due to the fact, that while the TSL photons can - and do - originate from the entire volume of the sample, only the electrons close to the sample surface can be efficiently extracted by the applied field. As the surface layer electrons are relatively rapidly depleted, those deeper in the solid layer have a greatly increased probability of recombining with positive "*holes*", rather than being able to attain the sample surface to be extracted and reach the electron detector. Obviously, similar argument can be made for the anomalous pressure rise, where the kinetic energy transfer - or the ballistic phonon propagation to the surface - will be more efficient for neutralizations occurring near the surface.

4.1.4. Summary

Our investigation of rare gas solids after exposure to electron beam using the methods of activation spectroscopy confirms that part of the energy of the high energy electrons (or photons) is stored in the solid in the form of defects, in the case of pure argon mainly self trapped Ar_2^+ holes, and electrons. Upon controlled heating of the sample, three dominant effects are observed: TSL VUV luminescence, emission of electrons or TSEE, and an anomalous rise in pressure, and our study demonstrates that their simultaneous monitoring on the same sample provides a better insight into the processes proceeding in the solid. In particular, comparison of experiments with linear and stepwise heating reveals a parallel behavior of the three effects and shows that they must be intimately intertwined, all caused by electron detrapping. The electrons thermally promoted into the conduction band neutralize the positive Ar_2^+ centers, emitting TSL photons in the VUV range, or if they are close to the surface, can be extracted and detected directly as an "$exo-electron$" current, TSEE. The energies bound-free VUV photons emitted by the argon dimers formed lie in a broad band centered around 9.7 eV, and are considerably lower than the total energy freed in the neutralization process. The remaining potential energy is converted into kinetic energy of the argon atoms and may then ballistically propagate long distances

through the lattice. Upon reaching the sample surface it may dislodge argon atoms, resulting in a measurable rise in pressure. Our investigation also indicates that there appears to be a nearly continuous distribution of electrons with different trapping energies, and with trap depths which change as the "*Coulombic landscape*" changes during the experiment.

References

[1] B. Meyer, *Low Temperature Spectroscopy*, American Elsevier Publishing Company Inc. New York, **1971**.

[2] *Molecular Ions: Spectroscopy, Structure and Chemistry*, Eds. T.A. Miller and V.E. Bondybey, North-Holland, Amsterdam, **1983**.

[3] *Chemistry and Physics of Matrix Isolated Species*, Eds. L. Andrews and M. Moskovits, North-Holland, Amsterdam, **1989**.

[4] V.A. Apkarian and N. Schwentner, *Chem. Rev.*, **1999**, *99*, 1481.

[5] V.E. Bondybey, M. Rasanen, A. Lammers, *Ann. Rep: Progr. Chem. C*, **1999**, *95*, 331.

[6] R.E. Johnson and J. Schow, *Mat. Fys. Med. K. Da. Vidensk. Selsk.*, **1993**, *43*, 403.

[7] E.V. Savchenko, A.N. Ogurtsov, E.V. Savchenko, A.N. Ogurtsov, S.A. Gubin, *Chem. Phys.*, **1994**, *189*, 415.

[8] E.V. Savchenko, A.N. Ogurtsov and G. Zimmerer, *Low Temp. Phys.*, **2003**, *29*, 270.

[9] E.V. Savchenko, A.N. Ogurtsov, I.V. Khyzhniy, G. Stryganyuk, G. Zimmerer, *PCCP*, **2005**, *7*, 785.

[10] D.R. Vij, in *Luminescence of Solids: Thermoluminescence*, Ed. D.R. Vij, Plenum Press, Ney York, **1998**, pp.271-307.

[11] M. Kirm and H. Niedrais, *J. Lumin.*, **1994**, *60*, 611.

[12] M. Kink, R. Kink, V. Kisand, J. Maksimov and M. Selg, *Nucl. Instrum. Methods B*, **1997**, *122*, 668.

[13] A. Schrimpf, C. Boekstiegel, H.-J. Stokman, T. Bornemann, K. Ibbeken, J. Kraft, and B. Herkert, *J. Phys.: Condens. Matter*, **1996**, *8*, 3677.

[14] A.N. Ogurtsov, E.V. Savchenko, O.N. Grigorashchenko, S.A. Gubin, and I.Ya. Fugol', *Low Temp. Phys.*, **1996**, *22*, 922.

[15] E.V. Savchenko, A.N. Ogurtsov, O.N. Grigorashchenko, S.A. Gubin, *Low Temp. Phys.*, **1996**, *22*, 926.

[16] E.V. Savchenko, O.N. Grigorashchenko, A.N. Ogurtsov, V.V. Rudenkov, G.B. Gumenchuk, M. Lorenz, A. Lammers, and V.E. Bondyney, *J. Low Temp. Phys.*, **2001**, *122*, 379.

[17] O.N. Grigorashchenko, V.V. Rudenkov, I.V. Khizhnyi, E.V. Savchenko, M. Frankowski, A.M. Smith-Gicklhorn, M.K. Beyer, and V.E. Bondybey, *Low Temp. Phys.*, **2003**, *29*, 876.

[18] E.V. Savchenko, O.N. Grigorashchenko, A.N. Ogurtsov, V.V. Rudenkov, G.B. Gumenchuk, M. Lorenz, A.M. Smith-Gicklhorn, M. Frankowski, and V.E. Bondybey, *Surface Review and Letters*, **2002**, *9*, 353.

[19] M. Frankowski, E.V. Savchenko, A.M. Smith-Gicklhorn, O.N. Grigorashchenko, G.B. Gumenchuk, and V.E. Bondybey, *J. Chem. Phys.*, **2004**, *121*, 1474.

[20] E.V. Savchenko and V.E. Bondybey, *Phys. Stat. Sol. (a)*, **2005**, *202*, 221.

[21] A. Cenian and H. Gabriel, *J. Phys.: Condens. Matter*, **2001**, *13*, 4323.

[22] V.D. Natsik, S.N. Smirnov, and Y.I. Nasarenko, *Low Temp. Phys.*, **2001**, *27*, 1295.

[23] E.V. Savchenko, G.B.Gumenchuk, E.M. Yurtaeva, A.G.Belov, I.V. Khizhniy, M. Frankowski, M.K. Beyer, A.M. Smith-Gicklhorn, A.N. Ponomaryov, V.E. Bondybey, *J. Luminescence*, **2005**, *112*, 101.

[24] E.V. Savchenko, O.N. Grigorashchenko, G.B. Gumenchuk, A.G. Belov, E.M. Yurtaeva, I.V. Khyzhniy, M. Frankowski, M. K. Beyer, A.M. Smith-Gicklhorn, and V.E. Bondybey, *J. Low Temp. Phys.*, **2005**, *126*, 621.

[25] K.S. Song and R.T. Williams, *Self-Trapped Excitons*, Springer-Verlag, Berlin, **1996**.

[26] E. Gullikson, *Phys. Rev. B*, **1988**, *37*, 7904.

4.2. Thermoluminescence in Solid Ar and Ne Samples Doped with Oxygen and Nitrogen

4.2.1. Introduction

An extended series of studies by Vegard [1–9] beginning in 1924 of cryogenic solids subjected to electron or X-Ray irradiation, and originally intended for investigations of atmospheric auroral emissions, opened the way for low temperature spectroscopy. More than twenty years later, Pimentel and coworkers realized that the low temperature solids are a suitable medium for studies of atoms, radicals, and other unstable and short lived species, and named the technique "*matrix isolation*". Much of the glow observed while irradiating solid nitrogen or nitrogen-containing rare gases was due to the doubly forbidden ^{2}D $\rightarrow ^4$S emission of nitrogen atoms produced by dissociating the molecules by electron impact, however molecular emissions are also observed. In particular, a extensive array of lines named by Vegard "$M-bands$", and known now be the so called Vegard-Kaplan $A^3\Sigma_u^+ \rightarrow X^1\Sigma_g^+$ band system of molecular nitrogen appeared strongly, and also weak emissions due to oxygen impurity, in particular the atomic ^{1}S$\rightarrow^1$D transition, were detected [10]. In their series of experiments Vegard and his co-workers studied N_2 spectra changing every conceivable parameter, including deposition temperature, effect of annealing, concentration, and presence of impurities. Vegard found that spectra vary with temperature and observed that at about 35.5 K n intense flash of light is emitted, with no emission being observed above that temperature.

The emissions resulting from irradiating solids containing nitrogen, and in particular the Vegard-Kaplan band-system, first detected by Vegard, were subsequently studied by a number of other investigators. In 1962, Brocklehurst and Pimental studied the mechanism of the glow and they explained it in terms of ^{4}S nitrogen atom recombination [11]. In 1968, Tinti and Robinson [12] performed

more detailed study of this system in rare gas matrices, and were able to detect and assign 67 vibronic transitions in the luminescence spectra of argon matrix, which made it at that time probably the best known and best studied system of any diatomic molecule. Compared with the gas phase, the solid phase bands were found to be "$red-shifted$", towards lower energies, and in addition to the Vegard-Kaplan system a so-called second positive system of molecular nitrogen, $C^3\Pi_u \rightarrow B^3\Pi_g$, was observed.

Also rare gas solids such as argon, krypton, or xenon containing oxygen were studied by several investigators, first in 1960 by L.J. Schoen and H.P. Broida [13], and later in 1978 by R.Smardzewski [14]. The former authors observed "$Herzberg\ I$" system, the $C^3\Sigma_u^+ \rightarrow X^3\Sigma_g^-$ transition while bombarding the samples by a beam of electrons. Also the oxygen lines were found to be significantly shifted in the rare gases, with the largest red shift of 941 cm^{-1} being detected in argon matrix. The latter author observed the "$Herzberg\ II$" system, $A^3\Sigma_u^+ \rightarrow X^3\Sigma_g^-$, during warm-up of O_3-contained solid inert gases previously photolyzed by UV light. The O_2 emission in this case was caused by ground state oxygen atom recombination in the course of the sample warm up.

In most of the above studies the observations were interpreted in terms of reaction of neutral atoms and radicals. However, irradiation of the samples with moderately high energy photons or electrons can also produce in the solids high concentrations of electrons and ionic species. Even in pure rare gas solids self-trapped ions, Rg_2^+, and electrons are produced. Only a relatively small amount of energy, supplied for instance by heating, is often needed to mobilize electrons in shallow "$traps$". This results in their promotion to the conduction band where they are relatively free to move around, and may recombine with some positively charged ions to producing neutral species in highly excited electronic states. While some of this excitation energy may be dissipated in the form of delocalized lattice phonons, the relaxation of the excited states may also result in emission of photons. The possible role of such charged species in the observed thermoluminescence was often not adequately considered. Only a relatively few recent studies [15–18] focused their

attention more closely on thermally stimulated reactions of charged species. One of the problems with the usual TSL experiments is the difficulty of establishing if the observed photons have their origin in neutralization of ions, or in recombination reactions of neutral species. As noted above, when electrons are promoted to the conduction band, they also may, before having the chance to neutralize positive ions, also leave the solid surface, and be detected as the so-called Thermally Stimulated Exo-electron Emission, TSEE. Clearly, observing simultaneously both effects, the TSEE current and the TSL light emission, should provide useful clues, and may help to a better understanding of the relaxation processes, and distinguishing between the relative contributions of neutral and ionic species.

4.2.2. Experimental details

The results presented here were obtained with the help of a new low-temperature experimental setup developed in our group and designed specifically for real-time correlated measurements of Thermally Stimulated Luminescence (TSL) and Thermally Stimulated Exo-electron Emission (TSEE) on the same sample. Since it is described in details in "*Experimental Setup*" section there is no reason to repeat it here. There will be a short description of the sample preparation and measurement procedure only given here.

To prepare the gaseous samples nominally pure Ar (99,999%), Ne (99,999%), N_2 (99,999%), and O_2 (99,998%) were used. The gaseous mixtures of argon and nitrogen (with a concentration of nitrogen of 1%), argon and oxygen (with the same concentration of oxygen as in case for nitrogen) and neon with nitrogen (the same concentration as in other two samples was used) were prepared in the gas handling system and then the samples were deposited as it is explained in "*Experimental Setup*" section. The base pressure in the vacuum chamber at low temperature was below 10^{-8} $mbar$. The deposition was adjusted using a Bronckhorst gas-flow controller set to a rate of 2 STP ml/min. The amount of sample deposited was independently controlled by observing the pressure drop in the gas-handling system. The typical sample thickness was about 100 μm.

During deposition the samples were exposed to irradiation by a 500 eV electron beam with a current density of 30 $\mu A/cm^2$. The electron source was a 2.2 V tungsten filament. After completed deposition, the electron beam was turned off, and the substrate rotated to the appropriate position for collecting the data (see "*Experimental Setup*"). The heating rate of the samples was adjusted to 3.2 K/min by Low Temperature Controller LTC 60. The substrate's temperature changes during the measurements were also recorded. The TSEE emission was detected by an Au-coated copper Faraday plate, and the current amplified by a FEMTO DLPCA 200 amplifier. The TSL spectra in range from 200 nm to 1100 nm were measured by a three-channel OceanOptics S2000 spectrometer. The time window was set to a most appropriate value which differed from sample to sample since the signal intensity depended on the matrix.

As the temperature of the sample was increased, the spectra were repetitively accumulated and stored. Using a specially developed program the TSL results were stored in a form of 3-dimentional (3-D) time (temperature) - wavelength - intensity array. The programs we developed for this experiment permitted then to display the data as a 3-D view, or display a cut through the 3-D surface perpendicular to the time (or temperature) axis, yielding a wavelength resolved spectrum at a given temperature, or a cut perpendicular to the wavelength axis, giving an intensity variation of a particular spectral line in the course of the sample warmup.

4.2.3. Results and discussions

Nitrogen in argon matrix A representative 3-D plot obtained during linear warm-up of a pre-irradiated ni-tro-gen-contained solid argon is presented in Fig. 4.2.1. Most of the observed spectral lines can be assigned, in agreement with the previous studies of Tinti and Eloranta [20], to atomic N ^{2}D$\rightarrow^4$S and molecular N_2 $A^3\Sigma_u^+ \rightarrow X^1\Sigma_g^+$ emissions, as well as to NO, a$^4\Pi \rightarrow$X$^2\Pi$ system. In the long lived Vegard-Kaplan phosphorescence both, "*cold*", $\nu' = 0$, and "*hot*" lines, $\nu' > 0$, can be identified, with the relative intensities of the hot and cold bands exhibiting an interesting variation with temperature, with two distinct maxima near 12 and 25 K,

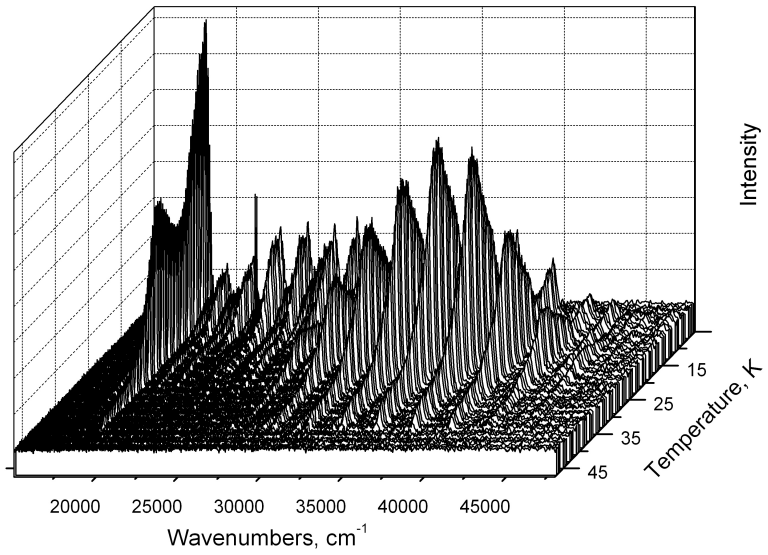

Fig. 4.2.1: A 3-D representation of the TSL spectra from solid Ar doped with 1% of N_2 while heating with 3.2 K/min rate

respectively. While at the lower, 12 K, temperature both the hot and cold Vegard-Kaplan bands are present, and also a strong O atom and intense NO emissions appear, the 25 K spectrum is much simpler, with only N atom and the cold, $\nu = 0$ Vegard Kaplan bands being present (see Fig. 4.2.2). A list of the spectral lines observed in TSL is given in Tab. 4.2.3. The lines' positions were determined by finding the maximum of the first derivative spectrum, representing the sharply rising high frequency (low wavelength) edge of the emission lines, which should most closely approximate the location of the zero phonon lines. Since, however, the resolution of the spectrometer is quite low, the accuracy of our line position measurements is rather poor.

The individual lines differ in the behavior of their intensities as a function of temperature. Based on similarities in their intensity profiles they can be clearly divided into several groups, and confidently assigned to specific carriers. These different profiles are exemplified in the Fig. 4.2.3, which shows the intensity-temperature data for several selected, well resolved representative spectral lines.

The most intense line in the spectrum, the $^2D \rightarrow {}^4S$ atomic nitrogen emission

Nitrogen Emission									NO Emission	
Molecular ($A^3\Sigma_u^+ \rightarrow X^1\Sigma_g^+$)									Atomic ^{2}D$\rightarrow^4$S	($a^4\Pi \rightarrow X^2\Pi$)	
ν‘	ν“	ν (cm^{-1})	ν‘	ν“	ν (cm^{-1})	ν‘	ν“	ν (cm^{-1})	ν (cm^{-1})	ν“	ν (cm^{-1})
0	2	44982	2	2	47717	4	8	37355	19119	4	30629
0	3	42688	2	3	45519	4	11	31151		5	28860
0	4	40438	2	4	43309	4	14	25191		6	27131
0	5	38256	2	6	38918	4	15	23309		7	25444
0	6	36061	2	7	36746	4	16	21398		8	23761
0	7	33941	2	8	34589	4	17	19535		9	22090
0	8	31803	2	10	30492(?)	4	18	17699		10	20474
0	9	29701	2	11	28443					11	18887
0	10	27618	2	12	26431	5	11	32445		12	17321
			2	13	24465	5	12	30492(?)			
1	2	46309	2	14	22493	5	16	22747			
1	3	44094				5	17	20846			
1	4	41888	3	11	27813						
1	5	39604	3	12	25844	6	14	27813			
1	7	35354	3	13	23882	6	16	24004			
1	8	33236	3	14	21913	6	18	20279			
1	9	31151	3	15	20058						
1	10	29073	3	16	18189						

Tab. 4.2.1: A list of the spectral lines observed in the TSL of the sample of solid Ar dopped with 1% of nitrogen

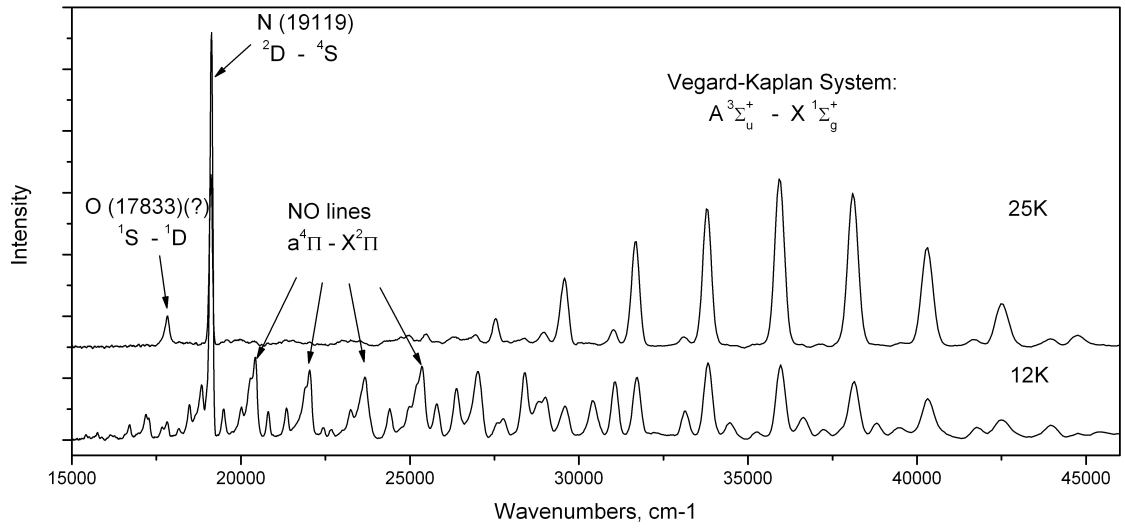

Fig. 4.2.2: The TSL spectra of solid Ar doped with 1% of N_2 taken at 12 and 25 K

at 19119 cm^{-1} is shown in the panel c. The signal starts rising sharply around 8 K, reaching its maximum around 12 K. The intensity then goes through a deep minimum centered around 19 K, before rising to a second, weaker maximum around 25 K. Above this maximum the intensity again decreases, and disappears completely around 43 K, probably close to the temperature where the sample is lost.

The panels a and b demonstrate the different behavior of the "*hot*" and "*cold*" Vegard-Kaplan lines, respectively. The cold, $\nu' = 0$ emission (represented by the 0-6 band) also exhibits, like the atomic line, two intensity maxima, however in this case the second, 25 K maximum is much more intense than the lower temperature, 12 K peak. On the other hand, the "*hot*" emission bands, (here the 1-9 band) exhibit quite different profiles, with the second, 25 K maximum being absent, and the intensity above 12 K only showing a gradual decrease to almost zero around 35 K.

The NO impurity is undoubtedly due to the formation of NO molecules as a result of the presence - and decomposition - of minor oxygen impurities, most likely H_2O, or traces of molecular O_2, and during the electron beam irradiation of the sample, emission of atomic oxygen is always observed. The TSL profile of the NO

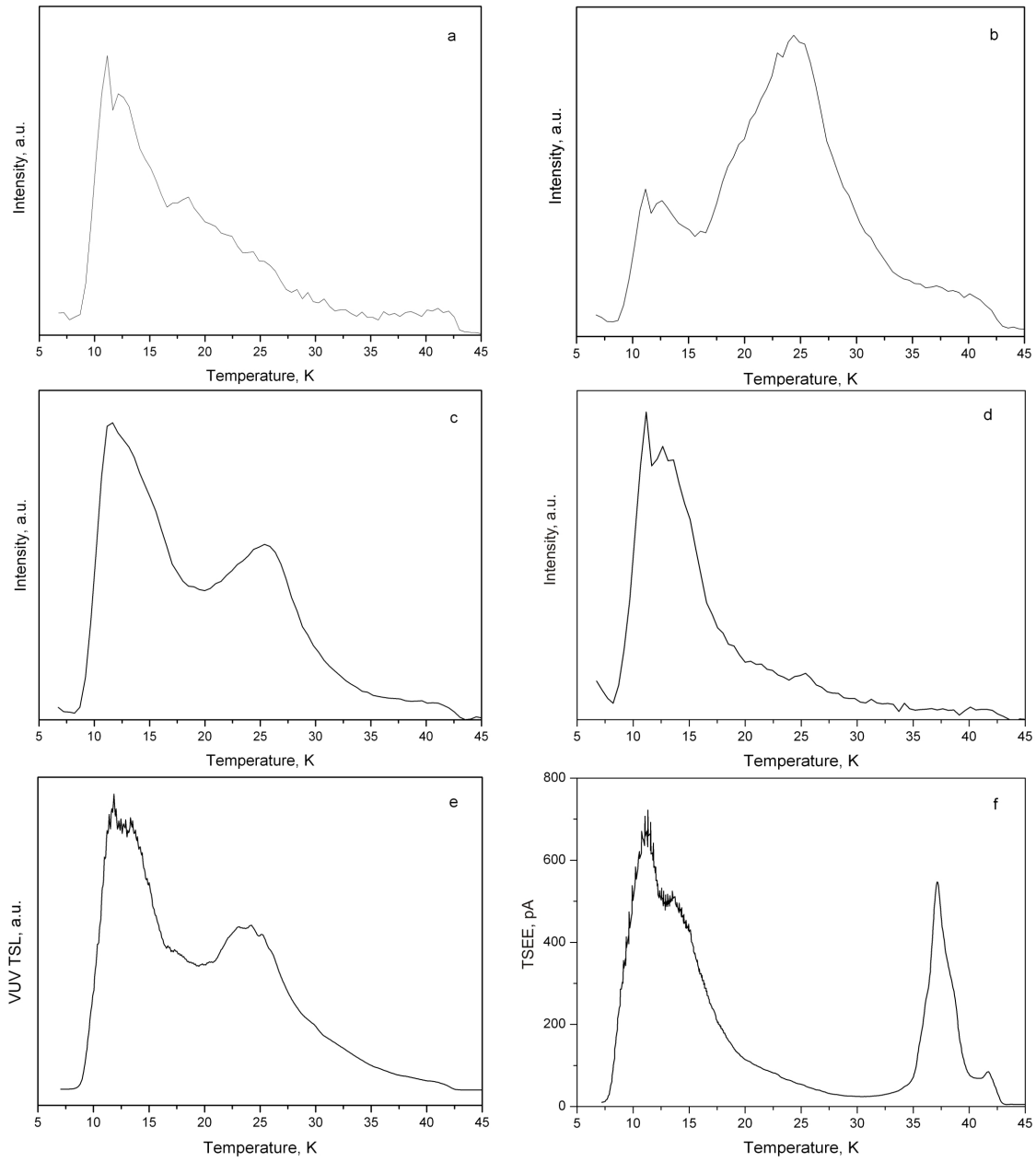

Fig. 4.2.3: The prifiles of the spectral lines observed in TSL spectra of solid Ar doped with 1% of N_2 (a - is the "hot'' molecular nitrogen emission, 31155 cm^{-1} with $\nu' = 1$ and $\nu'' = 9$, b - the "cold" molecular nitrogen emission, 36061 cm^{-1} with $\nu' = 0$ and $\nu'' = 6$, c - the atomic nitrogen emission, 19119 cm^{-1}, d - emission of NO, 22090 cm^{-1} with $\nu' = 0$ and $\nu'' = 9$), the VUV TSL emission of nominally pure solid Ar (panel e), presented in form of the Intensity vs.Temperature functions, and the TSEE curve (panel f) of nitrogen doped solid argon, taken simultaneously with TSL spectra

emission shown in the panel d exhibits also only the single, lower temperature maximum around 12 K, and drops then even more precipitously than the hot molecular N_2 emission.

For comparison with these data a sample of nominally pure Ar (99,999%) was deposited under the same conditions as mentioned above and the TSL measurements in VUV range as well as TSEE measurements were carried out. These results are presented in [19], here only the VUV TSL curve is given for comparison with the results on nitrogen-doped argon sample. It is shown in panel 3e.

The emission of electrons, TSEE in Fig. 4.2.3 f, appears around 8 K, and rises rapidly to the 12 K maximum with the line exhibiting possibly a relatively flat shoulder around 13-14 K, and decreases then rapidly to nearly zero above 20-25 K. A second sharp maximum appears around 37 K, corresponding again to the loss of integrity of the solid sample. Even though the exact profiles show minor differences, one can clearly see that each of the other signals in the Fig. 4.2.3 also exhibits a clear maximum around the same, 12 K temperature, and this provides a useful clue for the interpretation of the processes in the matrix. In the course of electron beam irradiation during sample deposition, numerous defects including impurities, vacancies, radicals, but also various ionic centers, and trapped electrons will be formed. Many of these electrons will be stabilized in various "*traps*" - vacancies, crystal defects and dislocations, or attached to various impurities present in the matrix. During the sample heating, the electrons may be released from the shallow traps and promoted into the conduction band. In case when the electron is located close to the surface it may completely escape the sample, giving rise to TSEE current. Most of these electrons, however, will not be able to escape, but will neutralize positively charged ions which are also present in the solid. The most common "*impurities*" in nominally pure solid rare gases after electron beam irradiation are the self-trapped ionic centers, effectively the rare gas ion dimers Rg_2^+, whose neutralization results in the extremely strong "*intrinsic*" VUV luminescence centered in solid Ar near 9.7 eV:

$$Rg_2^+ + e^- \rightarrow Rg_2^* \rightarrow Rg_2 + h\nu_1(VUV) \quad (4.2.1)$$

However, in the presence of impurities a variety of other cationic species will be formed in the solid, in matrices containing nitrogen mainly N^+ and N_2^+, and if traces of oxygen are present also NO^+. These ions can then also recombine with the conduction band electrons, giving rise to the observed visible and near UV bands:

$$N^+ + e^- \rightarrow N^* \rightarrow N + h\nu_2; \quad (4.2.2)$$
$$N_2^+ + e^- \rightarrow N_2^* \rightarrow N_2 + h\nu_3; \quad (4.2.3)$$
$$NO^+ + e^- \rightarrow NO^* \rightarrow NO + h\nu_4. \quad (4.2.4)$$

Examination of the Fig. 4.2.3 reveals clearly the similarity between the VUV luminescence in e and atomic nitrogen emission in c. This suggests that at least part of the atomic nitrogen signal may be due to re-absorption of the 9.7 eV VUV photons by the ground state N atoms.

Among the curves in the Fig. 4.2.3, the "*cold*" molecular N_2 emission in panel b stands out, in that here the strongest maximum occurs above 25 K, where essentially no TSEE is observable, suggesting that a different process should be responsible for the second maximum, and for the vibrationally relaxed emission. In solid argon, the 25-30 K temperature is known to be the approximate threshold, above which diffusion of atomic species may become efficient. In a solid, containing nitrogen atoms, their recombination may take place:

$$N + N \rightarrow N_2^* \rightarrow N_2 + h\nu_5. \quad (4.2.5)$$

Recombination of two ground state ^{4}S N atoms may, besides the ground state only form the lowest lying higher multiplicity states, in particular the $A^3\Sigma_u^+$. On the other hand, the recombination of ground state N_2^+ $X^1\Sigma_g^+$ dimer ions with electron will first populate very high lying Rydberg states of N_2 above 18 eV, which will then undergo a complex nonradiative relaxation cascade. It is this difference in the formation mechanisms at 12 K and 25 K which may explain the difference in the population of the excited state vibrational levels. Of course an alternative explanation for the absence of "*hot*" band emission at 25 K may be the increased rate of vibrational relaxation in the $A^3\Sigma_u^+$ at the higher temperatures. It should be noted, that the rather intense visible-near UV emission due to the reaction (4.2.5)

may also promote electrons from deeper traps into the conduction band, and thus contribute to the reactions (4.2.1-4.2.4). The intense Vegard-Kaplan emission due to the reaction (4.2.5) may thus contribute to the second maximum evident in the atomic N and cold N_2 emissions in Fig. 4.2.3 *c* and *e* occurring at a temperature of 25 K, where based on the TSEE curve in *f* most electrons in shallow traps - at least close to the sample surface - have already been depleted.

Oxygen in solid argon Results obtained with samples similarly doped with 1% of molecular O_2 and again irradiated during deposition by a 500 eV electron beam, are presented in the Figs. 4.2.4 and 4.2.6. The former figure shows a 3-D representation

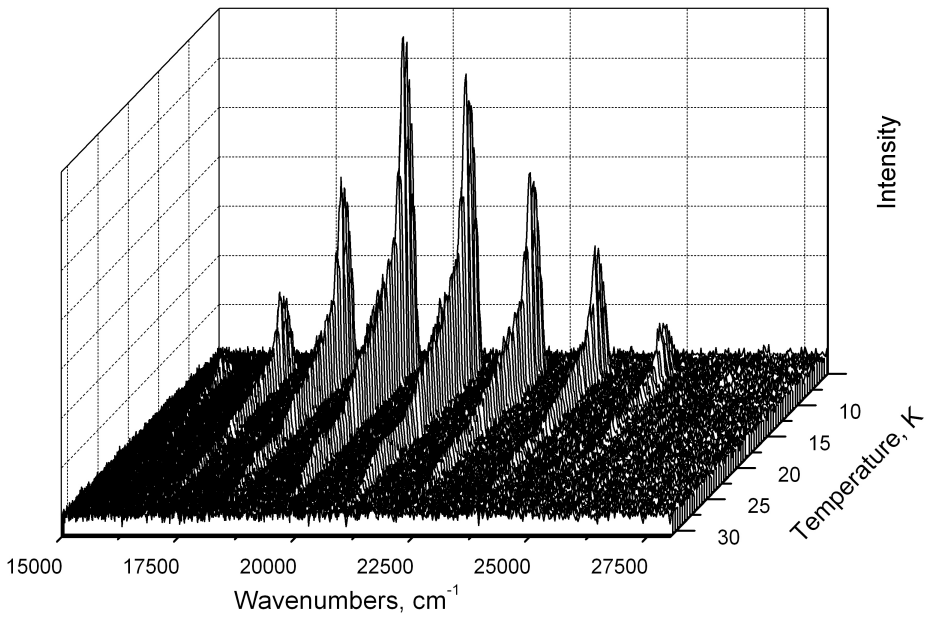

Fig. 4.2.4: A 3-D representation of the TSL spectra from the sample of solid Ar doped with 1% of O_2 during a heating with 3.2 K/min rate

of the TSL spectrum, where only vibrationally relaxed $A^3\Delta_u^+ \rightarrow X^3\Sigma_g^-$ transition of O_2, the so called Herzberg II bands, can be identified. The list of the spectral lines is given in Tab. 4.2.2, there is no sign of the $\nu' > 0$ hot bands. Fig. 4.2.5 and Fig. 4.2.6 then compare the variation of the TSL emission intensity as a function of temperature with that of the TSEE current. All the emission lines, exemplified

Oxygen Emission $(A^3\Delta_u^+ \rightarrow X^3\Sigma_g^-)$	
ν“	ν (cm^{-1})
7	15720
8	17000
9	18295
10	19618
11	20975
12	22325
13	23731
14	25150

Tab. 4.2.2: A list of spectral lines observed in TSL of solid Ar doped with 1% of O_2

in the Fig. 4.2.5 by the integrated intensity of the strongest line at 19618 cm^{-1}, originate from the same upper level, the $\nu' = 0$ $A^3\Delta_u^+$, and accordingly exhibit identical temperature dependence.

The intensity of the TSL also shows a striking similarity to the variation of the TSEE current, presented in the panel *b*. Both the emission intensity and the current appear around 8 K, the intensities go through a single maximum around 11 K, and then slowly decrease, disappearing almost completely above 25 K. Unlike the optical emission, the TSEE curve seems to suggest a second, relatively weak maximum around 37 K, again near the temperature where the solid sample is lost.

The similar behavior of the two signals clearly suggests that the two processes, electron emission and luminescence are closely related, suggesting that similar to the nitrogen results, the luminescence is a consequence of thermal promotion of trapped electrons into the conduction band. Apparently, the electrons mobilized by the sample heating neutralize the O_2^+ ions formed under irradiation by the electrons beam:

$$O_2^+ + e^- \rightarrow O_2^* \rightarrow O_2 + h\nu. \quad (4.2.6)$$

In comparison with the experiment with nitrogen in the argon samples doped with oxygen, no second, higher temperature maximum, which could be attributed to a diffusion and recombination of neutral oxygen atoms is detected. This may be

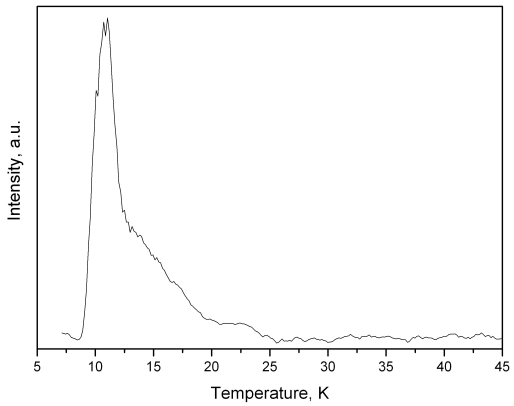

Fig. 4.2.5: The Intensity vs.Temperature profile of the most prominent spectral line of the molecular oxygen emission at 19616 cm^{-1}

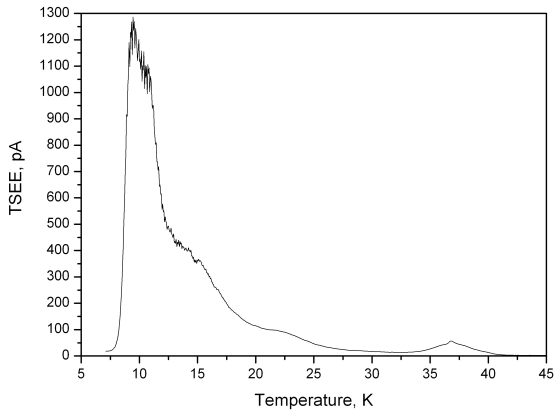

Fig. 4.2.6: The TSEE emission from the sample of solidified Ar doped with 1% of O_2

due to the positive electron affinities of oxygen, which is 2.6 eV for the O_2 molecules and 1.6 eV for atoms, which will form deep traps for the electrons. It is therefore possible that most of the available oxygen atoms attach during the sample irradiation electrons, so that concentration of neutral atoms remains low. The oxygen atoms formed from the molecule dissociation under electron bombardment serve as deep traps for the electrons. In this case the probability of the formation of negative ions O^- is very high.

Nitrogen in Solid Neon The TSEE curve for an irradiated neon sample doped with 1% of nitrogen is given in Fig. 4.2.7.

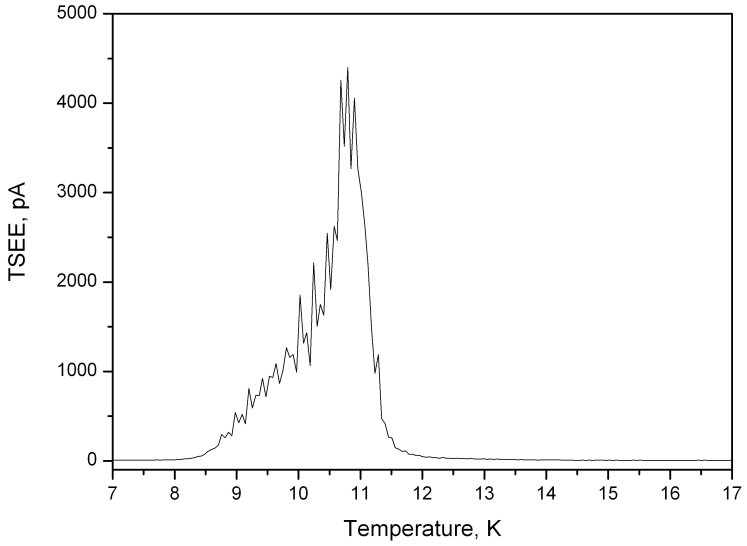

Fig. 4.2.7: The TSEE curve of solid Ne doped with 1% of nitrogen.

The emission of the electrons begins at 8.5 K, and seems initially to rise almost linearly with temperature, then rises more rapidly to a maximum around 11 K, and then drops precipitously, disappearing almost completely by 12 K. The TSL spectrum of the same sample is presented in a 3D form in the Fig. 4.2.8. The emission consists of vibrationally relaxed lines of the $A^3\Sigma_u^+ \rightarrow X^3\Sigma_g^+$ Vegard-Kaplan transitions, which are listed in the Tab. 4.2.3, the ^{2}D$\rightarrow^4$S atomic nitrogen line, and an additional line, probably due to the ^{1}S$\rightarrow^1$D atomic oxygen line.

The integrated intensities of some of this lines, atomic nitrogen line, molecular nitrogen line, and atomic oxygen line, in each of the spectrum versus temperature are given in Figs. 4.2.9 a, b, and c respectively. It is interesting that in comparison to argon sample in solid neon, the atomic and molecular nitrogen lines, panels a and b respectively, have very similar shapes and are characterized by only one maxima of the intensity nearly 11.5 K. Both lines start rising around 9 K, reach maximum near 11.5 K, then slowly decrease and around 15 K completely disappear. The intensity of the atomic oxygen line, panel c, changes differently. It increases starting

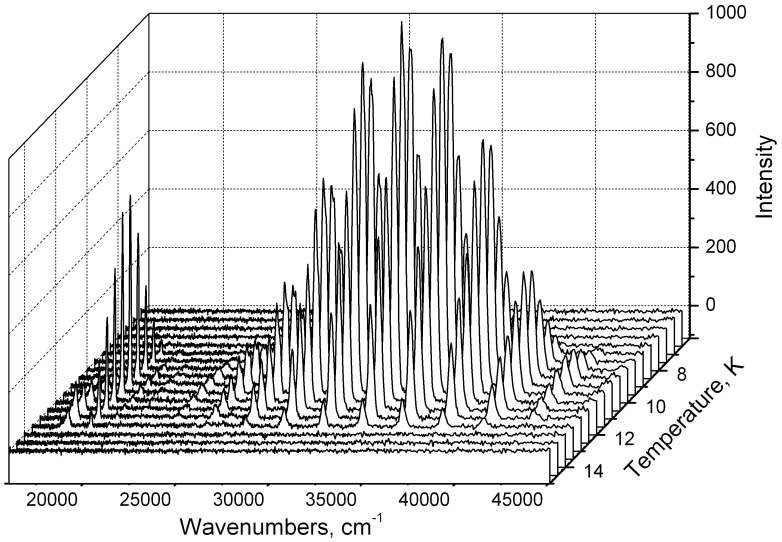

Fig. 4.2.8: A 3-D representation of the TSL spectra from solidified nean matrix doped with 1% of N_2. The heating rate was 3.2 K/min.

from nearly 10 K, goes up to its maximum around 13 K, and then drops down and disappears at 14.5 K.

To interpret these observations we can suggest that during sample preparation under electron bombardment a dissociation of nitrogen molecule occurs. Taking into account that the electron affinity of neon is negative and significantly higher then that's of argon the chances for stabilising ions, such as N^+ and N_2^+, may be rather low. However, a significant number of neutral atoms must be formed. During the warm-up procedure at certain temperature a diffusion of nitrogen atoms in a solid begins leading to reaction of atom-atom recombination:

$$N + N \rightarrow N_2^* \rightarrow N_2 + h\nu. \quad (4.2.7)$$

The N_2 luminescence emitted during this reaction can excite nitrogen atoms to the ^2D state whose relaxation back to the ^4S state results in the atomic nitrogen emission presented in the spectra. The intensity rise of the molecular and atomic nitrogen emissions are in a very good correlation what very nicely confirms the suggestions given above. Alternatively, the emission of light due to the reaction of N_2^+,

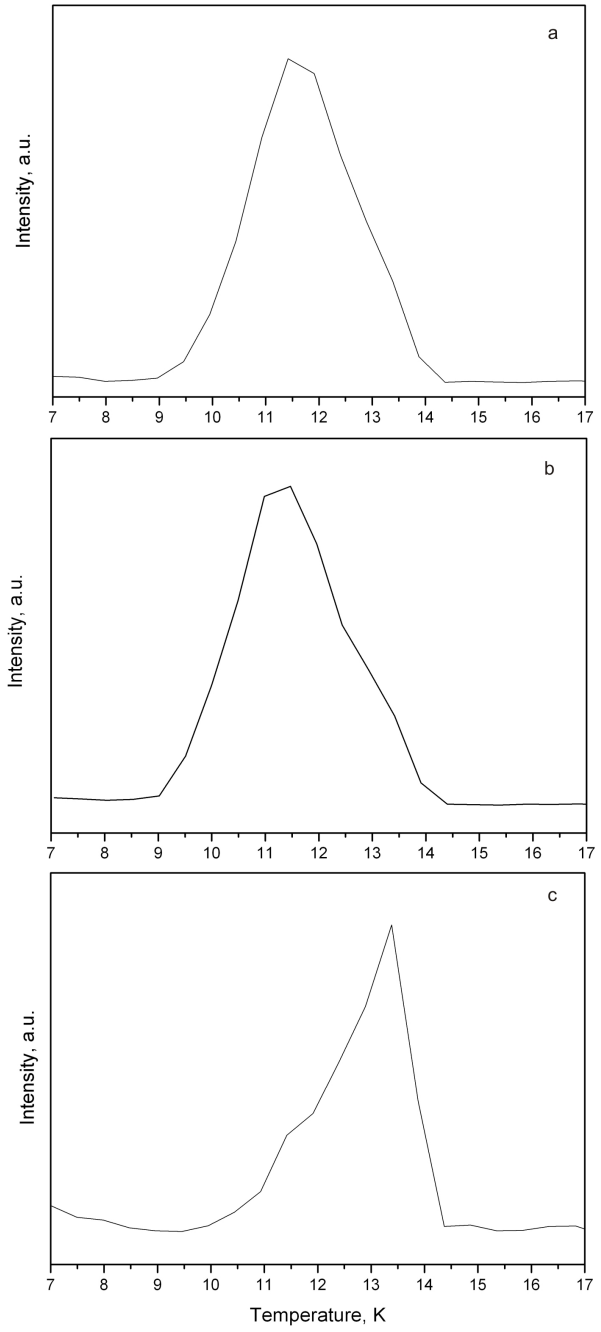

Fig. 4.2.9: The Intensity vs.Temperature profiles of the spectral lines of the different emissions observed in TSL of the solid Ne with 1% of N_2 (*a* - atomic nitrogen line, 19233 cm^{-1}; *b* - molecular nitrogen line, 33984 cm^{-1}; *c* - atomic oxygen emission, 17989 cm^{-1}.)

Nitrogen Emission			Oxygen Emission
Molecular ($A^3\Sigma_u^+ \rightarrow X^1\Sigma_g^+$)		Atomic (^{2}D$\rightarrow$ ^{4}S)	Atomic (^{1}S$\rightarrow$ ^{1}D)
ν“	ν (cm^{-1})	ν (cm^{-1})	ν (cm^{-1})
3	42757	19233	17989
4	40499		
5	38310		
6	36109		
7	33984		
8	31877		
9	29765		
10	27702		
11	25678		
12	23661		

Tab. 4.2.3: A list of the spectral lines observed in the TSL of the sample of solid Ar dopped with 1% of nitrogen

produced during sample preparation under electron bombardment, with electrons is located in the VUV range and the photon energies are also high enough to excite nitrogen atoms.

An experiment on relatively pure neon (99,998% purity) was performed and an intrinsic TSL emission of neon in VUV range was recorded. The glow-curve is presented in Fig. 4.2.10. The emission starts at 8.5 K, then the curve has two maxima of the intensities nearly 10 and 11 K, then it decreases and disappears around 13-14 K. It can be now seen that the atomic nitrogen emission is much better correlated with molecular nitrogen emission then with VUV emission of neon.

As it was mentioned above, in the TSL spectra an atomic oxygen emission was also detected. This is probably due to O^+ ions formed during the sample preparation under irradiation by the electrons, and their recombining with electrons released from traps during the sample warm-up. Since the concentration of oxygen in the sample is quite low (oxygen is presented as a residual gas in the vacuum chamber) and its electron affinity is positive, the probability for these ions or even neutral oxygen atoms to survive in the neon matrix is very low. This may account

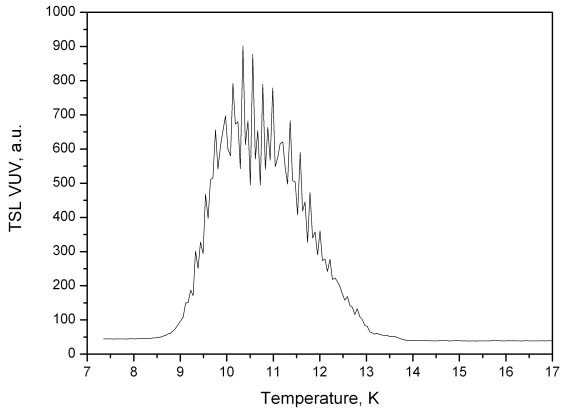

Fig. 4.2.10: The VUV TSL emission from nominally pure (99,998%) solid Ne

for the fact that there was no molecular oxygen emission observed. On the other hand, it might be present, but so week that the spectrometer was not able to detect it. We have also performed an experiment on solid neon doped with 1% of O_2, in this case, however, no TSL emission was at all observed. The measurements in the VUV range were not done.

4.2.4. Summary

In the manuscripts mentioned in the introduction, we have examined solidified rare gases doped with various molecular species, and exposed to ionizing radiation. The main attention there was paid to the role of neutral species in the Thermally Stimulated Luminescence, TSL process, observed during the controlled sample warm-up. The present work focuses more on ions and electrons, and presents a conclusive evidence that these charged species also play a very important role in the TSL emission. The key in providing this definitive evidence was the construction of a new, versatile experimental setup and the related software, which allow us to detect and monitor several related processes simultaneously, on the same sample. The new apparatus detects and monitors, in a time correlated manner, the TSL - either integrated, or spectrally resolved in the wide range of 200-1100 nm - and the TSEE current. The new data obtained here provided clear answers so several of the previously still open

questions.

References

[1] L. Vegard, *Nature*, **1924**, *114*, 357.

[2] L. Vegard et. al., *C.R. Acad. Sci.*, Paris, **1925**, *180*, 1084.

[3] L. Vegard, *Leiden Commun.*, **1925**, *175*.

[4] L. Vegard, *C.R. Acad. Sci.*, Paris, **1926**, *182*, 211.

[5] L. Vegard et.al., *Verlag Akad.*, Wetenschap., Amsterdam, **1927**, *36*, 364.

[6] L. Vegard, *Ann. Phys.*, **1930**, *6*, 487.

[7] L. Vegard et.al., *Commun. Phys. Lab.*, Univ. Leiden, **1930**, *205b*, 1949.

[8] L. Vegard, *Commun. Phys. Lab.*, Univ. Leiden, **1930**, *205a*, 3.

[9] L. Vegard, *Nature*, **1948**, *162*, 967.

[10] A.M. Bass, H.P. Broida, eds., *Academic Press*, New York, **1960**.

[11] B. Brocklehurst, G.C. Pimentel, *J. Chem. Phys.*, **1962**, *36*, 8.

[12] D.S. Tinti, G.W. Robinson, *J. Chem. Pys.*, **1968**, *49*, 3229.

[13] L.J. Schoen, H.P. Broida, *J. Chem. Phys.*, **1960**, *32*, 4.

[14] R.R. Smardzewski, *J.Chem.Phys.*, **1978**, *68(6)*, 15; *J. LTP* **2001**, *122*, 379.

[15] E.M. Fajardo, V.A. Apkarian, *J. Chem. Phys.*, **1988**, *89(7)*, 1.

[16] A. Schrimpf et.al., *J. Phys.: Condens. Matter*, **1996**, *8*, 3677-3689.

[17] E.V. Savchenko, V.E. Bondybey, *Phys. Stat. Sol.(a)*, **2005**, *202*, 221.

[18] J. Becker, O.N. Grigorashchenko, A.N. Ogurtsov, M. Runne, E.V. Savchenko, G. Zimmerer, *J. Phys. D: Appl.Phys.*, **1998**, *31*, 749-753.

[19] A.N. Ponomaryov, G.B. Gumenchuk, E.V. Savchenko, V.E. Bondybey, *Phys. Chem. Chem. Phys.*, **2007**, *9*, 1329.

[20] J. Eloranta, K. Vaskonen, H. Haekkaenen, T. Kijunen, H. Kunttu, *J. Chem. Phys.*, **1998**, *109*, 18.

5. Outlook and Summary

The current work presents new results of an investigation into radiation effects and relaxation processes involving charged and neutral species in "*pure*" and doped rare gas solids pre-exposed to a low energy electron beam. A set of activation spectroscopy methods was used to analyze the processes occurring in the solids during their warm-up. In order to monitor all relaxation processes under study simultaneously a new modification of low temperature activation spectroscopy technique was developed. The setup designed and special program permitted us to perform the real time correlated study of spectrally resolved thermally stimulated luminescence (TSL) in wide range of spectra, thermally stimulated exo-electron emission (TSEE) and ejection of particles from pre-irradiated cryogenic solids. The most important results may be summed up as follows:

- the synchronous measurements of TSL in the VUV range, TSEE and pressure above the surface of the sample demonstrated correlation in behavior of these phenomena. Both the linear heating as well as step-wise regime have shown a good correlation of the yields of the photon emission and emission of electrons, as well as a pressure rise in the sample vacuum chamber during activation of relaxation processes by heating of the sample. This proved the fact that all these processes have a common origin. It was found out that the initial process, triggering relaxation cascades is the thermally stimulated promotion of the electrons from shallow traps into the conduction band;

- analyzing data on kinetics, taken during step-wise heating of the sample, it was noticed that after each step of heating each signal, TSL, TSEE and pressure, were decaying following a double exponent. This suggests that during the heating at least tow processes in the sample are taking place: one is relatively fast, since its life time was in between 8-12 s, and the second one is rather slower with life times for each temperature step varied in range from 80 to 120 s. It was supposed that the first one is related to the electron detrapping and diffusion while the second one is probably due to atomic diffusion;

- the study of dose behavior of the TSL and TSEE yields demonstrated correlation in an increase of the total yield of VUV photons and total yield of TSEE under short exposures (between 1 min and 10 min), further irradiation resulted in more fast saturation of the TSEE yield than that of TSL. It was suggested that this is due to the fact that electrons can only be extracted from relatively thin surface layer of the sample;

- an additional proof of the "surface related" origin of TSEE phenomena was obtained in the experiments performed with variable electron energy and consequently variable penetration depth. Features in the TSEE yield were pronounced at low energy of an electron beam and an increase in TSEE yield with the energy rise was less distinct than that of TSL. In a course of these experiments generation of a negative space charge was found;

- the direct estimation of the TSEE active layer was obtained in the experiments with a variable sample thickness (samples were deposited under electron beam). While the TSL signal increased approximately linearly with time of sample deposition (and consequently sample thickness) there was no observable increase in the TSEE signal beyond about 10 min of the deposition, which corresponded to a sample thickness of just a few μm. This give an information about active layer for the emission of the electrons which can be detected;

- the experiment on the cycles of irradiation by the electrons - annealing - recooling of the same sample gave a good view on how the sample structure, changed from cycle to cycle, influences on TSL, TSEE and pressure above the sample. It was found that so-called "*anomalous low temperature desorption*" (desorption or ejection of own atoms from pre-irradiated matrix at temperatures much below characteristic sublimation point) is more effective when the structure is more perfect. An influence of the sample structure (number and distribution of electron trap) on TSL and TSEE yields and "structure" of the yields was demonstrated;

- the results obtained on the spectrally resolved TSL from solid Ar with dif-

ferent dopants (N_2 and O_2) permitted us to distinguish clearly between thermally stimulated reactions of charged and neutral species. Experiments were performed with simultaneous detection of TSL spectra in a wide range from 200 nm to 1100 nm. Pronounced changed in the intensity distribution of dopant spectral bands with temperature were found. Analysis of the vibrational structure of molecular series revealed qualitative differences in the intensity distribution at low and high temperatures. E.g. "*hot*" molecular bands (transitions from vibrationally excited states) of molecular nitrogen were detected at low temperatures and maximum of their intensity was observed at the same temperature as the yield of TSEE measured from the same sample. These findings suggest in a basis charge recombination reaction. In contrast at higher temperature only "*cold*" molecular bands emerged in the TSL spectra pointing to the thermally stimulated recombination of neutral species (N radicals). Using nitrogen and oxygen as dopants it was realized that the properties of dopants, such as electron affinity, are also of importance in a relaxation pattern.

6. Aknowledgements

Dear all with whom I have been working here the last three years and who has even a small contribution to this work!!! I would like to thank you for a good cooperation and nice time spent together. Without you my work here wouldn't become so interesting educational.

I want to thank Prof. Dr. V.E. Bondybey, my supervisor, for his ideas which are realized in this work and whose suggestions together with critical advices helped me to understand the experimental results taken in our laboratory and then to explain them in a suitable form for publication. His group provided an extremely creative, inspiring and international working environment.

I'd like to express my deepest "THANK YOU" to Prof. E.V. Savchenko, our co-worker from Verkin Institute for Low Temperature Physics and Engineering of the National Academy of Science of Ukraine and who actually was my co-supervisor, with whom all the experiments were done and who helped in analyzis of the results. Her knowledge lied to the basis of this work and lots of what I've got known in solid state physics is a result of the cooperation with Prof. E.V. Savchenko.

I should also say thanks to my former co-worker Dr. Marcin Frankowski, who is now working in Berlin, for his great cooperation in the lab and who actually introduced me into the group of Prof. V.E. Bondybey. Working with him in the lab was an interesting and educational event for me. Without him I'd not be able to understand anything in the lab.

Also I want to thank Dr. Alice M. Smith-Gicklhorn, who was our second coworker in "Matrix Isolation" group, for her help in the lab and who took care about me and my health in the first few months since I arrived to Germany.

My deep respect and thanks to Dr. Martin Beyer and Dr.Brigitte S. Fox-Beyer for very helpful scientific discussions and interesting talks during lunch times.

I shouldn't forget Mr."I need", Dr. Petru Balaj, for his advices in programming, nice time spent in beer-gardens and interesting excursion around Paris.

For a help with computer stuff and with technical questions I'd like to thank

Peter Kaemmerer and Matthias Stecher respectively who were always very kindly to do everything I needed.

I cordially thank Sabine Kullick, my teacher in German, and not only our secretary but also a "Lord of the documents" I always asked her to help with. Many thanks her for the help in correcting this dissertation as well.

Meantime I would very kindly to thank Galina Gumenchuk, our second PhD student, who is going to get a degree of Doctor together with me, and who always supported me in writing the dissertation and was taking care about the documents to have.

Of cause my deep "thank you" goes also to Mirko Gruber, a former diploma student in our group and who is currently a PhD student. Even though he is not a member of our group he is always ready to help any time it is needed.

For an opportunity to fill as a teacher in the lab during the time of "lab-classes" I want to thank Alexander Ogrodnik who is also very interesting and conversable interlocutor always ready to help if it's needed.

For an interesting time spent together I would like to thank also our other coworkers - Dr. Cheng Sun, Dr. Chi-Kit Siu and Dr. Julia Balteanu, who also took care about friendly and nice atmosphere in the group.

I should also thank Ivan Khizhniy, our coworker from Kharkov and who is actually a PhD student of Prof. E.V. Savchenko, for his "pressure" to visit very nice places in Bavaria and without whom I'd probably didn't do that.

I gratefully acknowledge the electronic and machine workshops for their excellent work and troubleshooting advice. Financial support by the Deutsche Forschungsgemeinschaft is gratefully acknowledged.

Finally I want to express my very-very DEEP THANKS to my parents - Liubov' I. Ponomaryova and Nikolay V. Ponomaryov, who gave me a birth and who supported me during the whole my life and whom I love so much, to my young brother Ivan, who was my best "enemy" in a childhood and whom I miss now so much, and to my young sister Maria, whom I am so proud of now and who became a real princes since I left my home-town.

7. Appendix A

7.1. The Program for Real-Time Correlated Measurements

To operate the complex new apparatus which allows simultaneous, real-time correlated measurements of TSEE, spectrally non-resolved VUV emission, as well as monitoring and recording the pressure in the vacuum chamber and the temperature of the substrate we have used a program, specifically written for this purpose. The program was developed with the help of a graphical programming interface LabView7.0. Rather than giving a full description of the rather complex program with many subprograms here, we will just present several screen-shots containing block-diagrams in which the main logic of the program is shown. We will then give a few comments on each of the block-diagram and use it to explain how the program functions.

7.1.1. The Measurements of the TSEE and VUV Signals and Monitoring the Temperatures of the Substrate and of the Cryostat

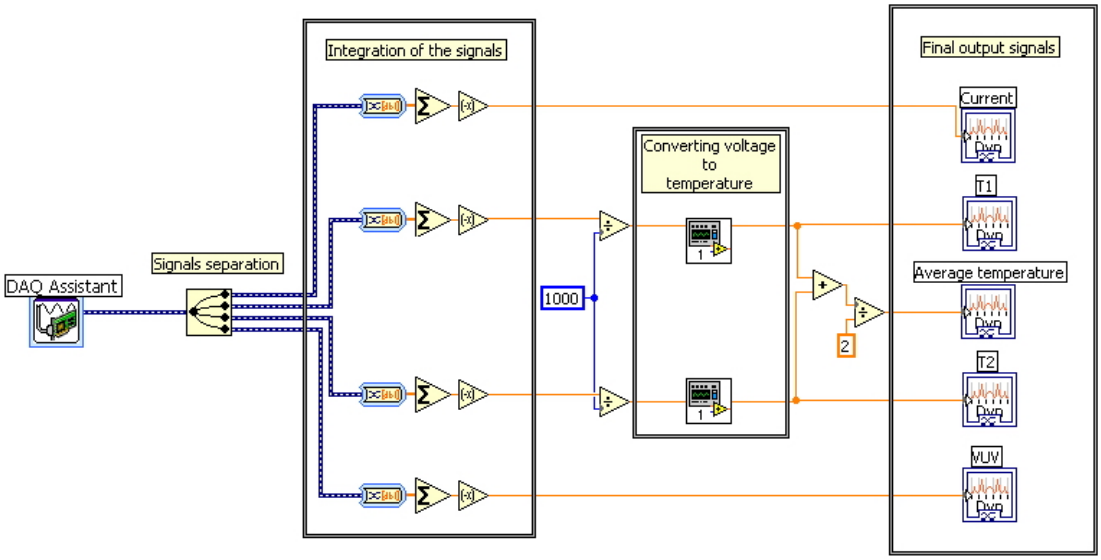

Fig. 7.1.1: Fig. 7.1: The block-diagram of the sub-program used for simultaneous time-correlated TSEE, VUV, cryostat and substrate temperatures

The Fig. 7.1.1 shows a block-diagram of the sub-program used for the TSEE and VUV measurements with simultaneous recording of substrate and cryostat temperatures. All of these signals are recorded and digitized by means of a Desktop BNC-2110 Adapter. This has 16 channels available, of which four are used in this experiment. A specific module called *DAQ Assistant* is used for communicating with the BNC adapter. In the adapter, the four analogue signals are digitized and come out as a digital signal which has to be decoded to separate the four digital signal values. Early testing of the program has revealed that measuring the TSEE, VUV and temperature signals every millisecond gave very noisy curves. For this reason the *DAQ Assistant* settings were adjusted to collect the signals measured every millisecond within a one second window to a single point in the *Integration of the signals* block. Obviously, in the case of temperature measurements, the integrated signals were then divided by 1000 (since within one second 1000 points were taken) to give an average value. This average the voltage value was then converted temperature by means of specially developed functions, which included the calibration data of the silicon diodes used as temperature sensors. Subsequently the temperatures were again averaged to obtain more precise value.

7.1.2. Monitoring of the Pressure in the Vacuum Chamber

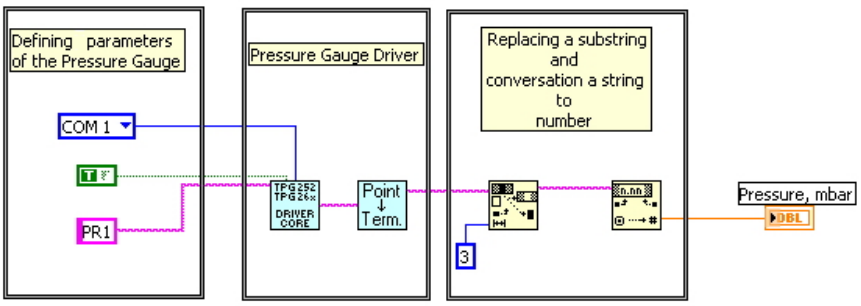

Fig. 7.1.2: The block-diagram of the sub-program used for the pressure measurements

The pressure measurements were performed with a help of Compact BA Pressure Gauge PBR 260 provided with a digital control unit with RS232 output. The PFEIFFER Company, who produced this pressure gauge, has also provided us a

specially designed driver for LabView. For the purpose of our experiment and for interfacing to our program the driver needed to be slightly modified, with the resulting modifications shown in the block-diagram in Fig. 7.1.2. In the *Defining parameters of the Pressure Gauge* block a port, write/read mode, and a sensor number are defined with *"ring constant"*, *"true constant"*, and *"string constant"* respectively. These parameters are then sent to a main part of the driver which is not changed. At the output the driver gives a string which is then modified (a part of it is replaced by means of *"Replace substring"* function) and converted to the fractional number (*"Fract/Exp string to Number"* function is used).

7.1.3. The Program for Linear Seating of the Sample

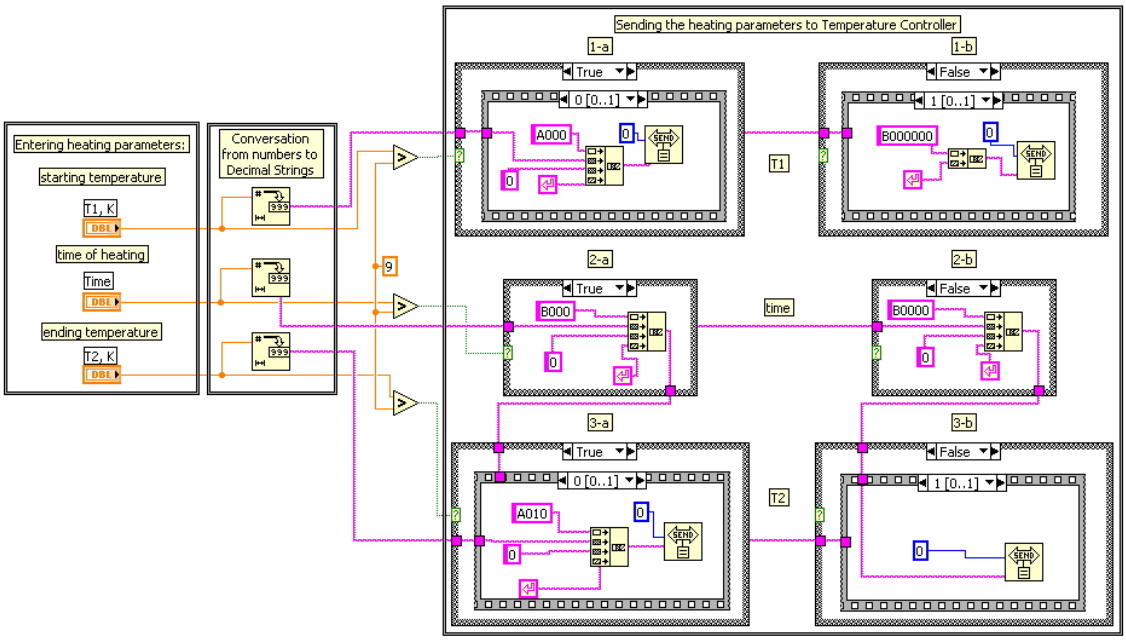

Fig. 7.1.3: The block-diagram of the sub-program used for the communication with Low Temperature Controller Leybold LTC 60 for the linear heating of the sample

As previously mentioned in the section *"Experimental setup"*, in order to control a heating of the sample a digital Low Temperature Controller Leybold LTC 60 was used. The controller is provided with a special key-pad, which allows entering a program for controlling the heating process. Depending on the heating regime the

number of steps to enter can vary in a very widely. For each temperature change the program requires three input parameters, a starting temperature, final temperature, and a time to perform this step. In the case of linear heating there are only three steps required: setting a starting temperature value, the desired temperature to heat to, and a time required for the step. On the other hand a step-wise heating regime used in many of our experiments requires a number of such steps. For each step one needs to set a certain temperature value and a time to reach it (usually it is set to 0, however, in practice it is needed to wait few seconds), then setting the same temperature value and a time to stay at it. The number of such steps can vary depending on the sample and on the temperature difference between two steps. For instance, in the case of solid argon heated in a step-wise regime with steps of $2K$ (see *"Radiation effects, energy storage and its release in solid rare gases"* section) there were up to 20 steps, and entering manually the input parameters for each step becomes quite awkward. In order to simplify this, as well as to avoid possible typing mistakes, it proved preferable to develop a program which would perform these functions automatically. A communication between temperature controller and computer was realized via a GPIB port. A block-diagram of the program for linear heating regime made in LabView 7.0 is given in Fig. 7.1.3 above. A program written for the stepwise is obviously different but it won't be described here in details.

Each of the parameters needed to be entered to the temperature controller has to be sent in form of a specially defined string. The string starts from a certain symbol which defines a command: a temperature value is going to be entered, or time value, or it is a command to run/stop heating. For example a command for the temperature value is defined like *"Axxnnnn ⟨cr⟩"*, where *"xx"* - is a step's number, *"nnnn"* - is a temperature value with one decimal digit, and *"⟨cr⟩"* - is ASCII *"Carriage Return"*. A command for time is defined by *"Bxxnnnn ⟨cr⟩"*.

In a program with a block-diagram presented above, first of all, three *"numeric controls"* (see block *Entering heating parameters*) are used to enter parameters of heating: *starting temperature*, *ending temperature*, *time of heating*, and *ending*

temperature. Then the numbers are converted to the decimal strings by *"Number to Decimal String"* function (*Conversation from numbers to decimal strings* block). Meantime, in order to not overcome a length limit of the command string (number having two digits is converted to a string of two symbols etc.) the numbers are compared to 9, function *"Greater?"*, which is the last one built of one symbol.

In the block *Sending the heating parameters to Temperature Controller* the command lines are built and then sent to the temperature controller. The functions *"Greater?"*, mentioned above are used also as switches for *"Case structures"*. The *"Case structures"* have two events, *"true"* and *"false"*, which are shown on different panels for better understanding. The panels marked with a belong to the *"true"* event while panels with b are of the *"false"* events.

The events of the *"Case structure"* used for *starting temperature*, panels $1-a$ and $1-b$, are very similar. They contain *"Stacked Sequence Structures"* with two frames. The command string for sending a temperature value of the first step is built in the first frame which is marked with 0. The command string for sending a time value for the same step is built in the second frame. In the both frames a *"Concatenate strings"* function is used. This function combines a string of several substrings and adds a *"Carriage Return Constant"* at the end. After the command string is completed it is sent to the temperature controller by a *"Send"* function via an address 0. In the second frame marked with 1 a command string for the time value (in a current case it equals 0 and a complete command is *"B000000 ⟨cr⟩*) is built and sent. The *"false"* event is similar to the *"true"* and differs only by a length of substring with temperature value which is shorter and compensated by an additional 0. That's why panel b presents a second frame of the *"Stacked Sequence Structures"*. In the cases of *Ending temperature*, blocks $3-a$ and $3-b$, the events in the *"Case structure"* are almost the same as for that of *Starting temperature*. The only difference is that the time command string is built from the *Time of heating* in a responsible *"Case structure"* shown on the panels $2-a$ and $2-b$, depending on the conditions mentioned above.

7.1.4. Step-Wise Heating of the Sample

For a step-wise heating procedure the program could be made on the same logic as for linear heating mentioned above. However, while testing the program it was found that the temperature controller developed unexpected problems and sometimes did not follow the program entered. The error occurred in a second step of the heating: the temperature difference was higher then it was needed. In a third step it was lower. Only in a fourth step the temperature controller worked according to the program. In order to avoid this problem it was decided to not program the controller but send to it a command to set a certain temperature after a certain time period defined by the experiment and which is constant during the whole heating procedure. The time period was set manually in the program before the heating process started. This program won't be described here since its block diagram it too complicated even tough that logically it is very simple.

8. Appendix B

8.1. List of Publications

1. **Anomalous low-temperature desorption from preirradiated rare gas solids**

   E.V. Savchenko, G.B.Gumenchuk, E.M. Yurtaeva, A.G.Belov, I.V. Khizhniy, M. Frankowski, M.K. Beyer, A.M. Smith-Gicklhorn, A.N. Ponomaryov, V.E. Bondybey.

   J. Luminescence, **2005**, *112*, 101-104.

2. **Oxygen-driven processes in pre-irradiated Ar cryocrystals**

   E.V. Savchenko, A.G. Belov, G.B.Gumenchuk, A.N. Ponomaryov, and V.E. Bondybey.

   Fizika Nizkikh Temperatur (Low Temperature Physics), Special Issue on Low Temperature Spectroscopy and Optics, **2006**, *32*, 1417-1425.

3. **Photo- and thermally stimulated relaxation processes in pre-irradiated atomic solids**

   E.V. Savchenko, I.V. Khyzhniy, G.B.Gumenchuk, A.N. Ponomaryov, M.K. Beyer, M. Frankowski, and V.E. Bondybey.

   Radiation Physics and Chemistry, **2007**, *76*, 577-581.

4. **Relaxation emission of electrons and photons from rare-gas solids: correlation and competition between TSL and TSEE**

   E.V. Savchenko, I.V. Khyzhniy, G.B.Gumenchuk, A.N. Ponomaryov, and V.E. Bondybey.

   Accepted for publication in *Physica Status Solidi*, **2007**.

5. **Photon-stimulated charge recombination and exoelectron emission from pre-irradiated solid Ar**

G.B. Gumenchuk, A.M. Bludov, A.G. Belov, A.N. Ponomaryov, V.E. Bondybey and E.V. Savchenko.

Accepted for publication in *Physica Status Solidi*, **2007**.

6. **Optically stimulated exoelectron emission from solid Ar irradiated by an electron beam**

   G.B. Gumenchuk, A.N. Ponomaryov, A.G. Belov, E.V. Savchenko, and V.E. Bondybey.

   Accepted to publication in *Fizika Nizkikh Temperatur (Low Temperature Physics)*, **2007**, *33*.

7. **Thermally stimulated exoelectron emission from solid Xe**

   I.V. Khyzhniy, O.N. Grigorashchenko, A.N. Ponomaryov, E.V. Savchenko, V.E. Bondybey.

   Accepted to publication in *Fizika Nizkikh Temperatur (Low Temperature Physics)*, **2007**, *33*.

8. **Thermoactivation spectroscopy of solid Ar doped with N2**

   A.N. Ponomaryov, E.V. Savchenko, G.B. Gumenchuk, I.V. Khizhniy, M. Frankowski, and V.E. Bondybey.

   Accepted to publication in *Fizika Nizkikh Temperatur (Low Temperature Physics)*, **2007**, *33*.

9. **Relaxation channels and transfer of energy stored by pre-irradiated rare-gas solids**

   E.V. Savchenko, I.V. Khyzhniy, G.B. Gumenchuk, A.N. Ponomaryov, and V.E. Bondybey.

   Submitted to *Radiation Measurements*.

10. **Radiation effects, energy storage and its release in solid rare gases**

    A.N. Ponomaryov, G.B. Gumenchuk, E.V. Savchenko and V.E. Bondybey.

PCCP, **2007**, *9*, 1329-1340

8.2. National and International Presentation

1. **"Protonated and fragment ions of acetonitrile. Mass-selective matrix-isolation study"**

   M. Frankowski, A.M. Smith-Gicklhorn, Zh. Sun, A.N. Ponomaryov and V.E. Bondybey.

   Fifth International Conference on Low Temperature Chemistry (LTC5), Berlin-Dahlem, Germany, September 7-10, 2004, p.72, poster.

2. **"Predictions of novel Xe compounds with BN"**

   A.M. Smith-Gicklhorn, M. Frankowski, A.N. Ponomaryov and V.E. Bondybey.

   Fifth International Conference on Low Temperature Chemistry (LTC5), Berlin-Dahlem, Germany, September 7-10, 2004, p.111, poster.

3. **"Relaxation Emission of electrons and photons from rare-gas solids: correlation and competition between TSL and TSEE"**

   E.V. Savchenko, I.V. Khyzhniy, G.B. Gumenchuk, A.N. Ponomaryov, and V.E. Bondybey.

   EURODIM 2006, 10th Europhysical Conference on Defects in Insulating Materials, July 10-14, 2006, Milano, University of Milano-Bicocca, Italy, p.103, oral talk.

4. **"Photon-stimulated charge recombination and exoelectron emission from pre-irradiated solid Ar"**

   E.V. Savchenko, G.B. Gumenchuk, M.O. Bludov, A.G. Belov, A.N. Ponomaryov, V.E. Bondybey.

   EURODIM 2006, 10th Europhysical Conference on Defects in Insulating Materials, July 10-14, 2006, Milano, University of Milano-Bicocca, Italy, p.343, poster.

5. **"Thermoactivation spectroscopy of solid Ar doped with N2"**

A.N. Ponomaryov, E.V. Savchenko, G.B. Gumenchuk, I.V. Khyzhniy, M. Frankowski and V.E. Bondybey.

CC 2006, Sixth International Conference on Cryocrystals and Quantum Crystals, September 3-7, Kharkov, Ukraine, P47, p.133., poster.

6. **"Optically stimulated exoelectron emission from solid Ar irradiated by an electron beam"**

   G.B. Gumenchuk, A.N. Ponomaryov, A.G. Belov, E.V. Savchenko and V.E. Bondybey.

   CC 2006, Sixth International Conference on Cryocrystals and Quantum Crystals, September 3-7, Kharkov, Ukraine, P48, p.135, poster.

7. **"Thermally stimulated exoelectron emission from solid Xe"**

   I.V. Khyzhniy, G.B. Gumenchuk, O.N. Grigorashchenko, A.N. Ponomaryov, E.V. Savchenko, V.E. Bondybey.

   CC 2006, Sixth International Conference on Cryocrystals and Quantum Crystals, September 3-7, Kharkov, Ukraine.

8. **"Relaxation channels and transfer of energy stored by pre-irradiated rare-gas solids"**

   E.V. Savchenko, I.V. Khyzhniy, G.B. Gumenchuk, A.N. Ponomaryov and V.E. Bondybey.

   LUMDETR 2006, 6th European Conference on Luminescent Detectors and Transformers of Ionizing Radiation, June 19-32, Lvov, Ukraine, Tu-P25-DM, p.124, poster.